END
DATE
FILMED
9-77
DDC

1.0

1.1

1.25   1.4   1.6

2.8   2.5
3.2   2.2
3.6
4.0   2.0

1.8

MICROCOPY RESOLUTION TEST CHART
NATIONAL BUREAU OF STANDARDS-1963

Technical Report 109

AN INTERNAL PHONON THEORY FOR THE THERMAL DEPENDENCE OF LINEWIDTH IN Nd^{+3} YAG

GC Mooradian
Atmospheric and Space Optical Communications Branch

25 April 1977

D D C

AUG 24 1977

C

**NAVAL OCEAN SYSTEMS CENTER
SAN DIEGO, CALIFORNIA 92152**

ADMINISTRATIVE INFORMATION

REPORT DOCUMENTATION PAGE		READ INSTRUCTIONS BEFORE COMPLETING FORM
1. REPORT NUMBER NOSC Technical Report 109 (TR 109)	2. GOVT ACCESSION NO.	3. RECIPIENT'S CATALOG NUMBER
4. TITLE (and Subtitle) AN INTERNAL PHONON THEORY FOR THE THERMAL DEPENDENCE OF LINEWIDTH IN Nd^{+3} YAG		5. TYPE OF REPORT & PERIOD COVERED Research and Development
		6. PERFORMING ORG. REPORT NUMBER
7. AUTHOR(s) GC Mooradian		8. CONTRACT OR GRANT NUMBER(s)
9. PERFORMING ORGANIZATION NAME AND ADDRESS Naval Ocean Systems Center San Diego, CA 92152		10. PROGRAM ELEMENT, PROJECT, TASK AREA & WORK UNIT NUMBERS 62762N; F54545; XF54545033 (NOSC F233)
11. CONTROLLING OFFICE NAME AND ADDRESS Naval Electronic Systems Command Washington, DC 20360		12. REPORT DATE 25 April 1977
		13. NUMBER OF PAGES 54
14. MONITORING AGENCY NAME & ADDRESS(if different from Controlling Office)		15. SECURITY CLASS. (of this report) UNCLASSIFIED
		15a. DECLASSIFICATION/DOWNGRADING SCHEDULE

16. DISTRIBUTION STATEMENT (of this Report)

Approved for public release; distribution is unlimited

17. DISTRIBUTION STATEMENT (of the abstract entered in Block 20, if different from Report)

AUG 24 1977

18. SUPPLEMENTARY NOTES

19. KEY WORDS (Continue on reverse side if necessary and identify by block number)

Lasers, optical communications, solid state, phonons

20. ABSTRACT (Continue on reverse side if necessary and identify by block number)

Since nonradiative processes affect such critical parameters in solid-state laser operations as linewidth of optical transitions and energy-level exchange, an understanding of the coupling between radiative and nonradiative processes is important. This document reports upon one aspect of this interaction by developing an internal phonon theory for the thermal dependence of linewidth in Nd^{+3} YAG.

The approach to the problem begins by first reviewing the energy levels and wave functions of rare-earth ions in crystalline hosts. This establishes notation and defines the wave functions which will be used later in nonradiative transition-rate calculations. The allowed radiative transitions are then briefly considered, primarily to introduce radiative selection rules which will be used later to determine the allowed lattice-assisted vibronic transitions (which

will determine not only the spectral range but also the validity of internal-mode interactions). The rigorous theory of phonons within a complicated crystal is then developed group-theoretically, analyzing the entire vibrational system. The coupling between the lattice and the active ion is subsequently considered with the single phonon process investigated rigorously. A nearest-neighbor approximation is then presented and the internal-mode formalism is developed. Here the parameters which determine the internal phonon interactions with the rare-earth ion are explicitly formulated and the number of interacting modes predicted. It is the prediction of the number of interacting modes which will make the internal mode approximation valid (via the vibronic spectra).

After completing the formal derivation of the direct phonon transition rate, the two-phonon Raman transition rate is derived, simplifying the expression where possible. The internal-mode approximation is then considered in detail and the vibronic transition rate is derived to determine the range of interacting phonons in the spectrum. A uniform phonon approximation for the "effective" modes is then proposed, which will determine not only the range of interacting modes but also the dominant broadening mechanism. Before applying this approximation to the broadening mechanisms, the Debye linewidth theory as presented by Yen, Scott, and Schawlow is reviewed. This is done primarily to place the proposed theory in proper perspective. Also, this furnishes a theoretical and historical base to the effective-mode theory to be presented. Derivation of the equations which will determine the functional form of the thermal variation of linewidth is pursued. Here the effects of all coupled modes are summed and analytic expressions are derived for each of the broadening mechanisms. Also, by employing the effective phonon spectrum, a dominant broadening mechanism can be predicted and the linewidth expressions greatly simplified.

With this formalism developed, the comparison of the predicted linewidth shape with the experimental data is investigated (data are available on transitions between multiplets of the $4F_{3/2}$ and $4I_{11/2}$ and $4I_{9/2}$). Only normalization to room temperature (determining a single multiplicative parameter) and determination of a low-temperature intercept (dependent upon sample quality) are necessary. The quality of the fit to the experiment is generally good and within the experimental accuracy. The sources of error (especially at elevated temperatures) are discussed and are consistent with those predicted, ie, second-order anharmonic effects are expected to degrade the agreement at high temperatures since the phonon theory employed is completely first order. Also, a breakdown of one of the approximations does occur due to the simplification made for the effective phonon spectra, wherein one set of energy levels exhibits an extraordinarily large direct phonon coefficient. This is not considered critical as inclusion of the neglected mechanism achieved very good agreement. Possible limits to the validity of the approximations made were indicated, and the trade-off of simplicity, predictivity, and consistency is significant.

OBJECTIVE

Since nonradiative processes affect such critical parameters in solid state laser operations as linewidth of optical transitions and energy level exchange, an understanding of the coupling between radiative and nonradiative processes is important. This technical report investigates one aspect of this interaction by developing an internal phonon theory for the thermal dependence of linewidth in Nd^{+3} YAG.

RESULTS

A simple, compact phonon mode theory predicting the shape of linewidth as a function of temperature has been developed. Only normalization to room temperature (determining a single multiplicative parameter) and determination of a low-temperature intercept (dependent upon sample quality) are necessary. The quality of the fit to the experiment is generally good and within the experimental accuracy. The sources of error (especially at elevated temperatures) are discussed and are consistent with that predicted, ie, second order anharmonic effects are expected to degrade the agreement at high temperatures since the phonon theory employed is completely first order. Also, a breakdown of one of the approximations does occur due to the simplification made for the effective phonon spectra, wherein one set of energy levels exhibits an extraordinarily large direct phonon coefficient. This is not considered critical as inclusion of the neglected mechanism achieved very good agreement. Possible limits to the validity of the approximations made were indicated, and the trade-off of simplicity, predictivity, and consistency is significant.

RECOMMENDATIONS

Expand this work to include other trivalent rare earths in other crystalline hosts.

ACKNOWLEDGEMENT

The author would like to acknowledge the professional encouragement and support given him by Dr Manuel Rotenberg of the University of California, San Diego during the development of this technical report.

1

CONTENTS

ILLUSTRATIONS

ILLUSTRATIONS (Continued).

INTRODUCTION

The physics of solid-state laser materials is well understood. Both time-independent and time-dependent problems, such as line positions and rate equations, have been investigated thoroughly. Interactions of the crystal lattice with an impurity ion is also fairly well understood, although not nearly as well as atomic phenomena. What is investigated much less frequently is the quantum electronics of the nonradiative processes, especially as it applies to the dynamic operation of solid-state lasers. Since nonradiative processes affect such critical parameters as linewidth and energy-level exchange, an understanding of the coupling between radiative and nonradiative processes is very important. The purpose of this report will be to investigate one aspect of this interaction by developing an internal dependence of linewidth of trivalent Neodymium (Nd^{+3}) in Yttrium Aluminum Garnet (YAG).

The system to be studied is simply an example of the general system of a rare earth ion replacing a constituent ion in a perfect crystal (Nd^{+3} replacing Y^{+3} in YAG). What is investigated about this system is the interaction between the impurity ion and the rest of the lattice and, in particular, how the radiative transitions are affected by nonradiative processes. The formulation of the coupling between the active ion and the surrounding lattice will determine how the lattice (ie, phonons) affects the rare earth ion. It is this interaction that broadens energy levels and spectrally broadens optical transitions. When the temperature dependence for the phonon occupation is included, the thermal dependence of linewidth may be derived.

In order to find the dominant broadening mechanism as well as the functional form of these interactions, the spectrum of those phonons affecting the active ion must be determined. In previous treatments, best illustrated by Yen, Scott and Schawlow[1,2,3,4], the Debye approximation was used, which considers only acoustic modes. This "external" mode theory is a poor approximation to what actually occurs, since lattice vibrations within the unit cells are ignored. The theory presented here departs from the previous treatments by considering only those optical phonons which couple strongly to the impurity ion; ie, those internal phonons resulting from nearest-neighbor interactions. This leads to a theory much different in intent as well as in functional form. The objective of the Debye-type theories is not to predict the shape of the linewidth-vs-temperature curve, nor even to formulate analytic expressions for the broadening mechanisms vs temperature, but rather to check the validity of the proposed broadening mechanisms themselves. The intent was never the formulation of a simple theory able to predict the shape of the linewidth-vs-temperature curves in trivalent, rare-earth doped crystals. This is the intent of this technical report: establish the internal mode formalism necessary to model the interactions; determine an approximation for the "effective" phonon spectra; using this approximation, derive compact expressions for the broadening mechanisms that do not require numerical integration nor the determination of nonmultiplicative parameters; employ approximations to simplify the formalism and determine the dominant broadening mechanism; and, finally, to attempt to predict the shape of the linewidth-vs-temperature curves for the transitions on which data are available. The comparison to experimental results will be found to be within experimental accuracy of the data, and sources of error are to be examined.

The approach to the problem begins by first reviewing the energy levels and wave functions of rare-earth ions in crystalline hosts. This establishes notation and defines the

[1] W Smith and P Sorokin, The Laser, McGraw-Hill Book Company, 1966
[2] WM Yen, WC Scott, and AC Schawlow, Physical Review, 136, A271, 1964
[3] DE McCumber and MD Sturge, Journal of Applied Physics, 36, 1682, 1963
[4] A Kiel, Physical Review, 126, 1292, 1962

wave functions which will be used later in nonradiative transition-rate calculations. The allowed radiative transitions are then briefly considered, primarily to introduce radiative selection rules which will be used later to determine the allowed lattice-assisted vibronic transitions (which will determine not only the spectral range but also the validity of internal-mode interactions). The rigorous theory of phonons within a complicated crystal is then developed group-theoretically, analyzing the entire vibrational system. The coupling between the lattice and the active ion is subsequently considered with the single-phonon process investigated rigorously. A nearest-neighbor approximation is then presented and the internal-mode formalism is developed. Here the parameters which determine the internal phonon interactions with the rare-earth ion are explicitly formulated and the number of interacting modes is predicted. It is the prediction of the number of interacting modes which will make the internal-mode approximation valid (via the vibronic spectra).

After completing the formal derivation of the direct phonon transition rate, the two-phonon Raman transition rate is derived and the expression is simplified where possible. The internal mode approximation is then considered in detail and the vibronic transition rate is derived to determine the range of interacting phonons in the spectrum. A uniform phonon approximation for the "effective" modes is then proposed which will determine not only the range of interacting modes but also the dominant broadening mechanism. Before applying this approximation to the broadening mechanisms, the Debye linewidth theory as presented by Yen, et al, is reviewed.[2] This is done primarily to place the proposed theory in proper perspective. Also, this furnishes a theoretical and historical base for the effective-mode theory to be presented. Derivation of the equations which will determine the functional form of the thermal variation of linewidth is now pursued. Here the effects of all coupled modes are summed and analytic expressions are derived for each of the broadening mechanisms. Also, by employing the effective phonon spectrum, a dominant broadening mechanism can now be predicted and the linewidth expressions greatly simplified. With the formalism developed, the comparison of the predicted linewidth shape with the experimental data is investigated. Only normalization to room temperature (determining a single multiplicative parameter) and determination of a low temperature intercept (dependent on sample quality) are necessary. The quality of the fit to the experiment is generally good and within the experimental accuracy. The sources of error (especially at elevated temperatures) are discussed and are consistent with those predicted, ie, second-order anharmonic effects are expected to degrade the agreement at high temperatures since the phonon theory employed is completely first order. Also, a breakdown of one of the approximations does occur due to the simplification made for the effective phonon spectra wherein one set of energy levels exhibits an extraordinarily large direct phonon coefficient. This is not considered critical as inclusion of the neglected mechanism achieved very good agreement. Possible limits to the validity to the approximations made were indicated, and the trade-off of simplicity, predictivity, and consistency is significant.

SUMMARY OF BROADENING MECHANISMS

If one is to formulate the effects of the phonon interactions and derive the phonon-photon equations, one must first understand non-radiative interactions. This will lead to an understanding of the thermal dependence of linewidth. Let us now briefly review some of the physics involved. The width of a transition (linewidth) is affected by four mechanisms, each having a different temperature dependence.[2] First is the mechanism of random microscopic strain within the host. Since the statistical variation in a crystal field on the impurity

6

ion results in a variation of the Stark splitting, we expect a Gaussian broadened line that should be temperature independent.[3,4]

The widths of radiative transitions (although ions vibrate rapidly) exhibit no Doppler broadening because the amplitude of vibration is so small. If ions have very short lifetimes in a particular state, then Heisenberg broadening will give rise to homogeneous Lorentzian lines having widths proportional to the total transition rates of each level. Consider the typical energy level scheme encountered with a rare-earth ion in a crystal (figure 1). Here we find groups of crystal field split Stark levels for each spin-orbit multiplet which are characterized by $2S+1_{L_J}$ (energy levels in rare earths will be examined later). Consider the state $|\psi_i\rangle$. The total transition rate, W_{tot}, both radiative and nonradiative, upward or downward to Stark levels within the J manifold or to other J manifolds, determines the homogeneous linewidth (full width, half maximum)

$$\Delta \nu \cong \frac{W_{tot}}{\pi} .$$

Since the radiative lifetimes are typically on the order of 10^{-2} to 10^{-6} second, we can be sure that this is negligible with regard to the observed linewidths. An understanding of the mechanisms of nonradiative energy level interactions will thus lead to the thermal variation of linewidth and to an understanding of the energy level exchange during the operation of a laser.
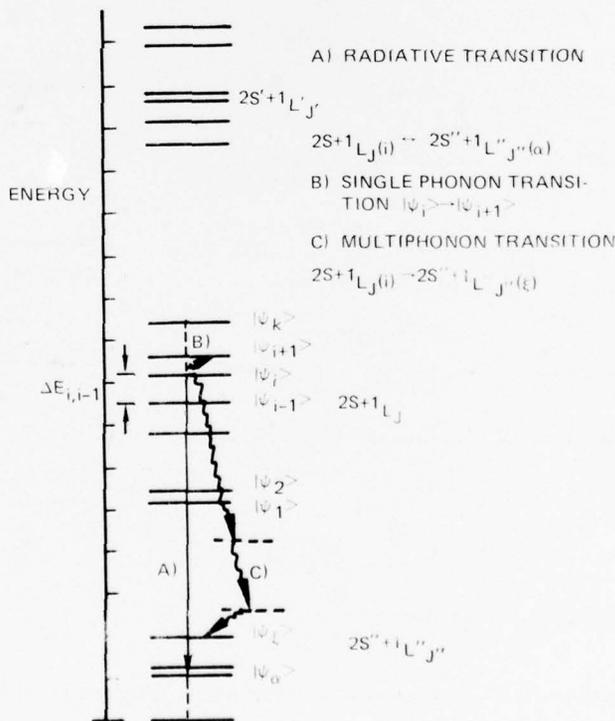
Figure 1. A typical energy level diagram for a rare-earth impurity ion in a crystal, showing both radiative and nonradiative transitions.

If there are phonons in the lattice resonant with the spacing of two ionic energy levels, then the lattice may couple with the ionic states and a direct, single phonon, non-radiation transition may occur either by phonon absorption or emission (figure 2). We will show later that W_d^D and W_u^D (the downward and upward direct transition rates) behave like:

$$W_d^D \propto [n(\omega) + 1] D'(\omega)$$

$$W_u^D \propto n(\omega) D'(\omega), \tag{1}$$

where $n(\omega)$ is the occupation number for phonons of frequency ω, the thermal occupation number is

$$n(\omega) = [\exp(\hbar\omega/kT) - 1]^{-1},$$

and $D(\omega)$ is the effective density of states for the ion-lattice system. The energy level spacing of the system of Stark levels is typically 10^1 to 10^3 cm^{-1} which results in transition rates

DIRECT UPWARD TRANSITION W_u^D

RAMAN UPWARD TRANSITION W_u^R

MULTIPHONON TRANSITION (P PHONONS OF ENERGY Δ) W_d^{mp}

DIRECT DOWNWARD TRANSITION W_d^D

RAMAN DOWNWARD TRANSITION W_d^R

COMPLICATED MULTIPHONON TRANSITION W^{mp}

* VIRTUAL OR INTERMEDIATE STATES
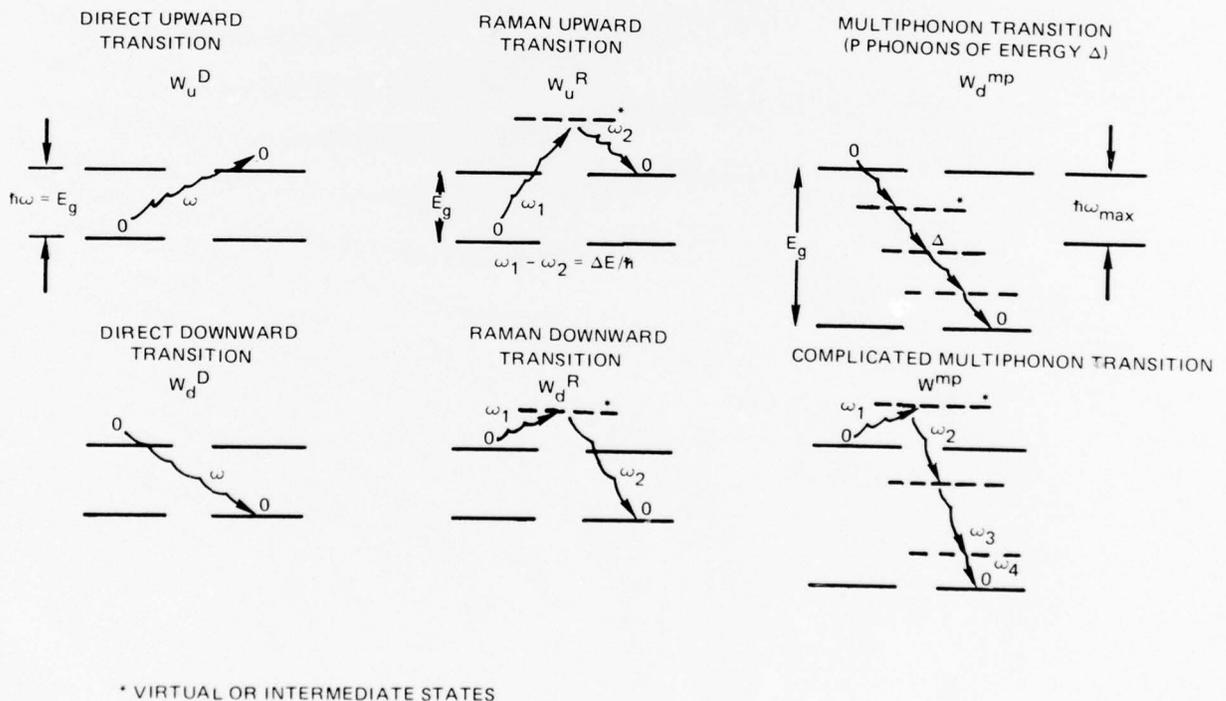
Figure 2. Illustrations of the phonon broadening mechanisms involving nonradiative transitions.

8

from $|\psi_i\rangle$ of about 10^{-11} second which results in levels ~ 3 cm^{-1} wide. Therefore, if the transition rates are summed for interactions with all the other levels, the total transition rate from $|\psi_i\rangle$ can be determined and, hence, the width of $|\psi_i\rangle$. If the same is done for $|\psi_\alpha\rangle$, then the width of the optical transition from $|\psi_i\rangle$ to $|\psi_\alpha\rangle$ may be determined. The phonon dependence, and therefore the temperature dependence, of that linewidth is then known.

If the level spacing is such that $\hbar\omega > \hbar\omega_{max}$, where ω_{max} is the largest frequency phonon supported by the lattice, then a higher-order process must be invoked, one which involves the emission and absorption of many phonons. In general, the multiphonon relaxation rate goes down as the order of the process, so in the energy conservation equation $\Delta \times p = E_g/\hbar$, we try to minimize p and still have Δ contained in the phonon spectrum where p is the number of phonons (order of the process), E_g is the energy gap, and Δ is the phonon frequency (figure 2). Thus, we would expect a simple expression of the form

$$W_d^{mp} \propto [\, (n(\Delta) + 1)\, D'(\Delta)\,]^p$$

(2)

$$W_u^{mp} \propto [\, n(\Delta)\, D'(\Delta)\,]^p \qquad (5, 6, 7, 8)$$

for the downward and upward multi phonon transition rates. The probability of a more complicated process requiring phonons of many frequencies could also occur because of the shape of $D'(\omega)$, selection rules, and so on. Since W^{mp} is a function of the occupation number n for phonons Δ, it has a temperature dependence and is in contradiction to the article by Yen.[2] Approximate temperature independence is achieved only when n is small compared to 1 in equation (2). Because Δ is large, n is small at all but the highest temperatures. It is important to note that it is this process which empties the thermal level to the ground state in Nd^{+3} YAG. The emission of two ~ 600-cm^{-1} phonons account for the 0.5-μs decay time from the thermal state. Therefore, while the multiphonon process contributes little to the linewidth broadening, it is very important in the exchange of energy levels (especially the thermal level depopulation).

The remaining broadening mechanism involves a second-order process which predominates at higher temperatures, the Raman-like scattering of phonons from impurity ions (eg, a Nd^{+3} ion replacing the Y^{+3} ion in YAG). This can be thought of as an absorption of one phonon and the emission of another with the difference frequency corresponding to the energy gap of the transition.[2] For a decay process we find the transition rate between levels separated by ΔE ($\omega_2 - \omega_1 = \Delta E/h$) is just

$$W_d^R \propto D'(\omega_1) n(\omega_1) \times D'(\omega_2)[n(\omega_2) + 1].$$

(3)

where ω_1 and ω_2 are the frequencies of the phonons (figure 2). We can see that, while at low temperatures $n \to 0$ and so does W^R, at high-temperatures W^R can become the predominant effect; the n's increase and many more phonons can contribute since all that is required

[5] WD Portlow and HW Moos, Physical Review, 157, 252, 1967
[6] CA Riseberg, WB Handrud, and HW Moos, Physical Review, 159, 262, 1967
[7] CA Riseberg and HW Moos, Physical Review Letters, 19, 1423, 1967
[8] CA Riseberg, HW Moos, and WD Portlow, Journal of Quantum Electronics, QE-4, 609, 1968

is that $\omega_2 - \omega_1 = \Delta E / \hbar$. Therefore, the total transition rate is summed for all interacting phonons in the spectrum.

Even from this brief description, the importance of knowing the detailed density of states, $D'(\omega)$, is obvious. For example, we know that the phonons which cause Raman-like relaxations are those where the difference between two peaks in $D'(\omega)$ corresponds to the transition energy. $D(\omega)$ is also important in determining the order of the multiphonon process, and so on. The use of the Debye acoustic-phonon model is common in deriving linewidth expressions but is actually a very poor approximation to what occurs. In the following sections a more correct expression will be used which limits the phonon spectrum to only those optical phonons which couple strongly to the impurity ion. This results in a reduction in the importance of the direct process and simplifies the Raman expression. Finally, a linewidth expression is derived which fits the experimental results to within a few per cent, within the stated experimental accuracy.

TRIVALENT RARE EARTHS IN CRYSTALLINE HOSTS

ENERGY LEVELS AND WAVE FUNCTIONS

The treatment of a rare-earth impurity ion located in a crystalline host is very complicated. In order to begin to understand the quantum electronics of selection rules, phonon transitions, and ion-lattice effects in general, a good understanding of ionic-energy levels and wave functions is required. This section reviews the necessary physics and establishes notation to be used later. The system of a Nd^{+3} ion located in a Y^{+3} site in YAG is used as an example; the formalism necessary to handle general ion-host combinations is similar.

Atomic Nd is number 60 in the periodic table and has a configuration of XENON $+ (4f)^4 (5d)^0 (6S)^2$. The normal oxidation state of rare earths is the trivalent state which results in a ground-state configuration for Nd^{+3} of XENON $+ (4f)^3 (5d)^0$. This is not the only possible configuration but merely the lowest-energy one. Other possible configurations are $(4f)^2 (5d)^1$, $(4f)^2 (6S)^1$, both having even parity. The importance of higher-energy configurations becomes clearer if parity-forbidden electric-dipole transitions are investigated.

Yttrium Aluminum Garnet has a chemical composition $Y_3 Al_2 (Al O_4)_3$ which is composed of body-centered cubic cells. The arrangement of the 80 ions which compose the unit cell is described by the space group symmetry. The local field (or that which is seen by the Nd^{+3} ion) is described by the point group symmetry; in this case, D_2 (or 222 in international notation). D_2 symmetry is that of three mutually perpendicular rotations of π (note figure 3). Notice that the crystal does not have inversion symmetry and, therefore, parity will not be a good quantum number. When this ion-host combination is used as a laser material, the Nd^{+3} ions are substituted into Y^{+3} sites at approximately one atomic per cent. Larger doping levels reduce the validity of a single-impurity ion approximation in the lattice (physically we get ion-ion effects which have macroscopic effects such as reducing the radiative quantum efficiency and inducing crystal strain).

The Hamiltonian of the Nd^{+3} ion in the crystalline site may be written as

$$H = \sum_{k=1}^{N} \frac{P_k^2}{2m} - \sum_{k=1}^{N} \frac{Z e^2}{|\bar{r}_k|} + \sum_{i>j=1}^{N} \frac{e^2}{|\bar{r}_i - \bar{r}_j|} \tag{4}$$

D_2	E	Q	C_2 QC_2	$U^{(2)}_{2(2)}$ Q U_2	$U^{(1)}_{2(1)}$ Q U_2
A	1	-1	1	1	1
B_3:x	1	-1	-1	-1	1
B_1:z	1	-1	1	-1	-1
B_2:y	1	-1	-1	1	-1
E′	2	-2	0	0	0
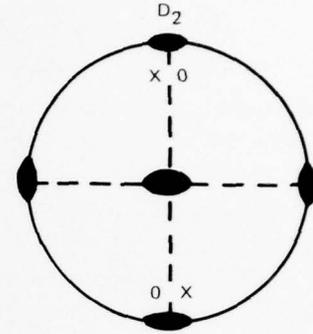
Figure 3. Character table of the irreducible representations for the crystal double group D_2 and the stereographic projection of the D_2 point group.

$$+ \sum_{k=1}^{N} \xi(\bar{r}_k) \, \bar{\ell}_k \cdot \bar{s}_k + H_{crystal}. \tag{4}$$

The first term is the kinetic energy of the N electrons, the second the electron-nuclear attraction, the third the electron-electron coulomb repulsion, the fourth the spin-orbit interaction, and the last the static effect of the lattice. Here, we also have $\bar{r}_k$ as the position of the kth electron, $\xi(r_k)$ as the spin-orbit coefficient, and N = 57, Z = 60. Since direct determination of the eigenvalues of H is impossible, successive applications of first-order degenerate perturbation theory is used. In very simple terms, we divide up the ionic parts of H as follows:

$$H^{(0)} = \sum_{k=1}^{N} \left[-\frac{h^2}{2m} \nabla_k^2 + V(r_k) \right]$$

$$H_{es} = - \sum_{k=1}^{N} V(r_k) + \sum_{i>j=1}^{N} \frac{e^2}{|\bar{r}_i - \bar{r}_j|} - \sum_{k=1}^{N} \frac{Z e^2}{|\bar{r}_k|}$$

$$H_{so} = \sum_{k=1}^{N} \xi(\bar{r}_k) \, \bar{\ell}_k \cdot \bar{s}_k . \tag{5}$$

11

$H^{(0)}$ (in the central field approximation) determines the electronic configuration, $(4f)^3$, and the starting wave functions. This configuration is 364-fold degenerate with respect to m_ℓ and m_S. The electrostatic perturbation H_{es} has the effect of adding the individual ℓ's and s's and results in wave functions described as $|\xi\, L\, S\, M_L\, M_S>$ with $\bar{L} =$

$$\sum_{k=1}^{N} \bar{\ell}_k,\ \bar{S} = \sum_{k=1}^{N} \bar{s}_k \text{ and } \xi \text{ designating all the other quantum numbers of the}$$

configuration such as the n and ℓ designation of (4f). Formally, the procedure is to find a vector space of functions composed of linear combinations of the old symmetrized wave functions $|n_a\, \ell_a\, m_{\ell_a}\, m_{s_a} >\ |m_b\, \ell_b\, m_{\ell_b}\, m_{a_b} > \cdots$ which diagonalize H_{es}. Thus, H_{es} splits the 364 degenerate levels into different levels depending upon L and S (the terms). Each term is still $(2L+1)(2S+1)$ fold-degenerate with respect to M_L and M_S.

The application of the spin-orbit perturbation H_{so} results in the vector addition of $\bar{L}$ and $\bar{S}$; where formally we say that the terms are diagonalized in the space $|\xi\, L\, S\, J\, M_J >$,

with $J = \sum_{k=1}^{N} (\bar{\ell}_k + \bar{s}_k)$. Now the wave functions are only $(2J+1)$ degenerate with

respect to M_J.

The validity of applying the perturbations in this order (the LS coupling scheme) is confirmed spectroscopically (figure 4), where we find that $H_{es} \sim 10,000\ cm^{-1}$, $H_{so} \sim 1,000\ cm^{-1}$, and $H_{crystal} \sim 100\ cm^{-1}$. Thus, we expect a given term, labelled by ^{2S+1}L, to be split by spin-orbit coupling into a close group of levels which are still characterized by L and S (to a good approximation) and distinguished by different values of J, noted by $^{2S+1}L_J$. The reduction of the $(2J+1)$ degeneracy is accomplished by the static Stark-effect term, $H_{crystal}$. The fact that the ion interacts only weakly with the crystal lattice is due to the small spatial extension of the (4f) wave functions. Likewise, this will be responsible for narrow spectra from transitions lying wholly within the $(4f)^3$ configuration (whereas interconfigurational $(4f)^3 \rightleftharpoons (4f)^2\, 5d$ transitions are characteristically much broader).

The application of the $H_{crystal}$ perturbation term turns out to be much more difficult. Although a brute-force diagonalization within the $(2J+1)$ ionic manifold is certainly possible, mathematical inconveniences render it impractical. Instead, by using the essential property of the crystal, namely symmetry, and the group theory, the determination of the qualitative splitting due to the crystal potential is greatly simplified. More important though, the transformation properties of the wave functions are determined which allow phonon selection rules, ion-lattice effects, and the like to be systematically studied.

In YAG, with the Nd^{+3} ion located in the low site symmetry D_2, all except the residual two-fold Kramer degeneracy is removed. The character table of the crystal double group derived for the nonintegral J's is given by figure 3.[9]

Since the purely ionic H is spherically symmetric, we find that the symmetry of the total H is that of $H_{crystal}$. In this group theoretical notation, it is determined that all wave functions are described by a two-dimensional E representation within the crystal double group D_2. For example, the main laser line is the transition $(4f_{3/2})_2\, E \rightleftharpoons (4I_{11/2})_3\, E$ (the 2 means the second Stark level from the bottom). It is only because of the low-point group

[9] W Chang, Principles of Quantum Electronics, Addison-Wesley Publishing Company, Reading, MA, 1969
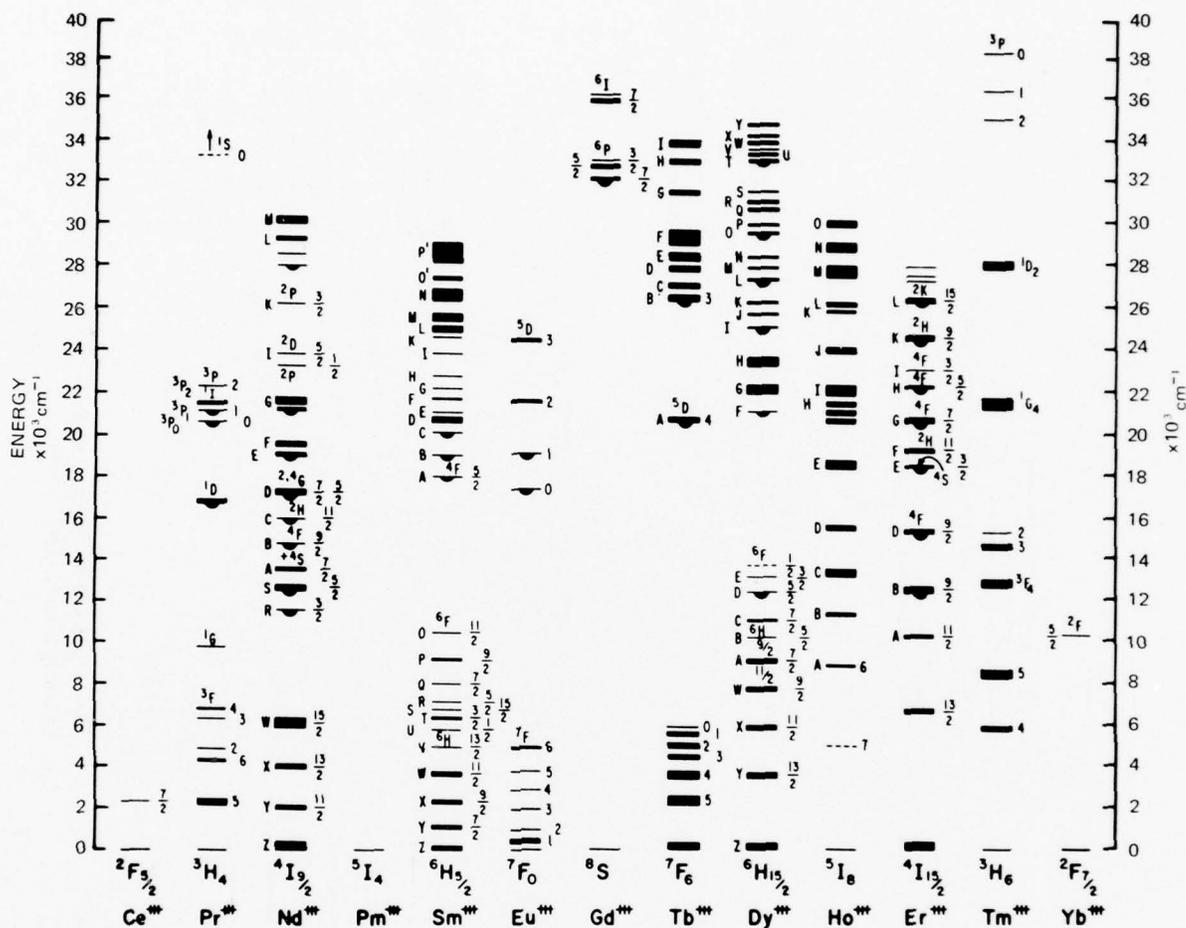
Figure 4. Observed energy levels of the trivalent rare-earth ions.[5]

symmetry that we have all energy levels transforming the same; in general, different wave functions corresponding to different states will transform differently under operations of the group and retain degeneracies.

Although group theory is very powerful, it cannot give the amount of Stark splitting (matrix elements must still be found). The techniques for calculating quantitative splitting are not discussed here.[6] The energy levels of Nd^{+3} YAG are given in figures 5 and 6.

ALLOWED RADIATIVE TRANSITIONS

Transitions between these levels are responsible for the operation of these materials as lasers. While the calculation of radiative transition rates for rare earths is actively pursued,[10],[11]

[10] GS Ofelt, Journal of Chemistry and Physics, 37, 511, 1962
[11] WF Krupke, Journal of Quantum Electronics, QE-7, 1953, 1971

14,919
14,826
14,797
14,689
14,638

$4F_{9/2}$ ~6700Å

13,633
13,594
13,570
13,563
13,435
13,371

~7400Å $4F_{7/2} + 4S_{3/2}$*

12,873
12,820
12,621
12,605
12,572
12,517
12,427
12,369

~7700Å $2G_{9/2}$

~8100Å $4F_{5/2}$

858 cm^{-1} TO $4F_{3/2}$
METASTABLE LEVEL

NOTE: DATA TAKEN AT 4.2° K

Figure 6. Some of the lower lying excited states forming the long wavelength
pumping bands for Nd^{+3} YAG.

848

311

197

134*

0

$4I_{11/2}$ (Z)
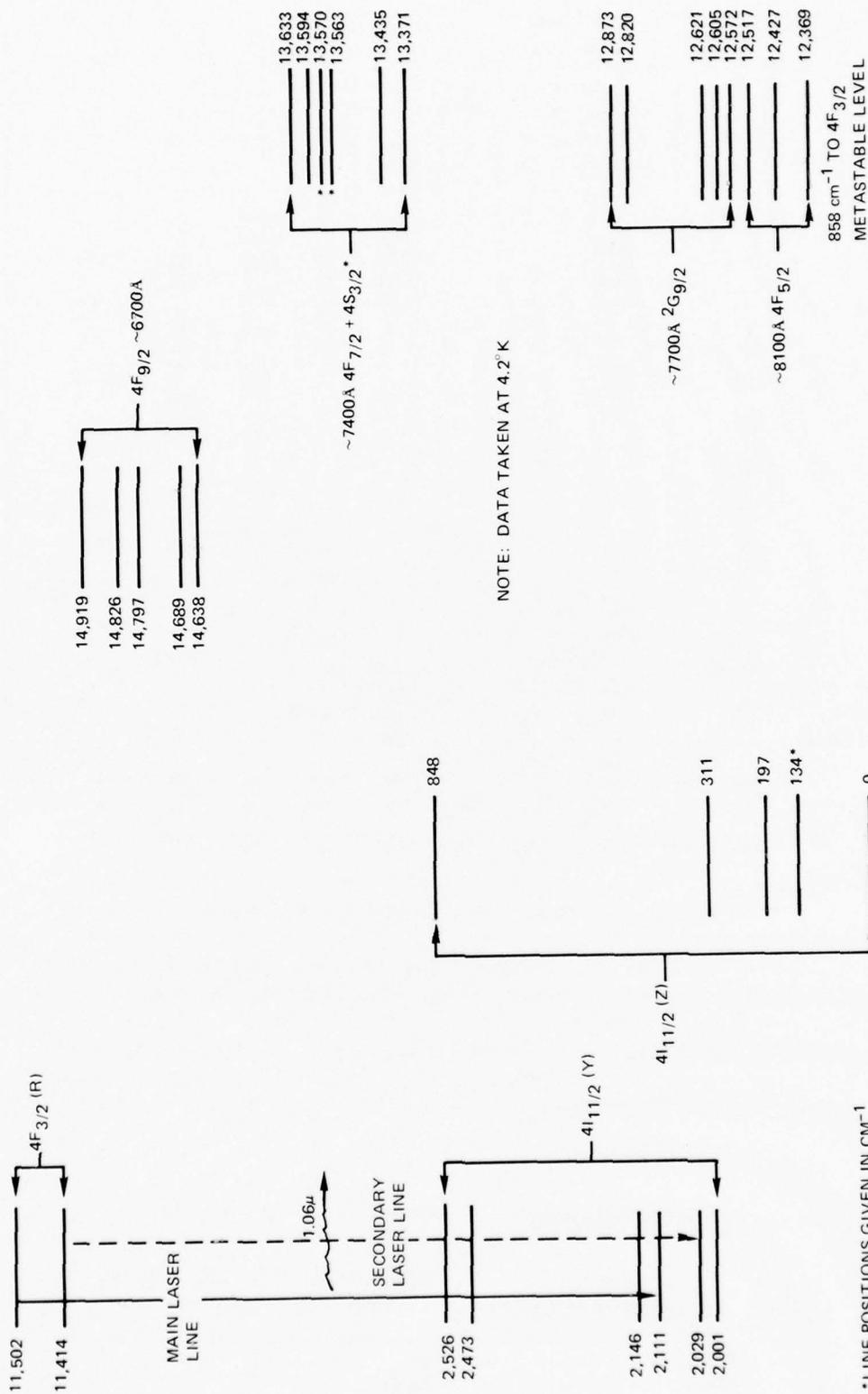
Figure 5. Relevant laser energy levels for Nd^{+3} YAG.

$4F_{3/2}$ (R)

1.06μ

MAIN LASER
LINE

SECONDARY
LASER LINE

$4I_{11/2}$ (Y)

11,502
11,414

2,526
2,473

2,146
2,111
2,029
2,001

*LINE POSITIONS GIVEN IN CM^{-1}

14

only a brief review will be presented here. The observed spectra of RE ions consist mainly of electric dipole transitions[1,10] which are governed by matrix elements of the type $\langle f \mid -e\, \vec{r} \mid i \rangle$. If the initial and final states $\mid i \rangle$ and $\mid f \rangle$ have the same parity (as with crystals having inversion symmetry and for transitions taking place wholly within the 4f shell) the electric dipole transition is rigorously forbidden. Only if there are odd parity terms in the static crystal potential or if there are odd parity vibrations to admix opposite parity states (eg, wave functions derived from the excited $(4f)^2$5d configuration) can electric dipole transitions occur.[10,12,13] We will assume here that only the odd terms of the crystalline potential can cause mixing of parity states and that the vibrational contribution is small (later we will use the weak vibronic emission and absorption spectra to determine the range of interacting phonons).

As stated before, the total electronic Hamiltonian is $H_{el} = H_{free\ ion} + H_c$, with

$$H_c = -e \sum_i V_c (r_i, \theta_i, \phi_i),$$

$V_c (r_i, \theta_i, \phi_i)$ being the crystal field potential at the i-th (4f) electron (in our example the summation extends over the three (4f) electrons of Nd^{+3}). It is often convenient to expand H_c in spherical harmonics

$$H_c = \sum_n \sum_{m=-n}^{n} \sum_i A_n^m\ r_i^n\ Y_n^m (\theta_i, \phi_i), \tag{6}$$

where the A_n^m coefficients are constants determined by the position of the neighboring ions around the central RE ion (ie, point-group symmetry), r_i^n refers to the radius of the i-th (4f) electron and the $Y_n^m (\theta_i, \phi_i)$ are spherical harmonics. This potential may be separated into even and odd parity parts (with n even and odd respectively) and written as

$$H_c = H_c \text{ (even)} + H_c \text{ (odd)}.$$

In the calculation of line positions, only the even terms of H_c are important and, therefore, the odd spherical harmonics are ignored. Since the Stark splitting involves matrix elements such as $\langle \psi_{free\ ion} \mid H_c \mid \psi_{free\ ion} \rangle$, we need only consider terms in H_c with $n \leq 6$ (since the f electrons with $\ell = 3$ cannot connect states with $n > 3 + 3 = 6$).[14]

Analogous results are obtained when calculating transition rates. Here we will require matrix elements between admixed states such as $\langle f \mid -e\, \vec{r} \mid \chi \rangle$, with

$$\mid \chi \rangle = \mid i \rangle + \frac{\sum_\beta \langle \beta \mid H_c \text{ (odd)} \mid i \rangle \mid \beta \rangle}{E_i - E_\beta}, \tag{7}$$

where the summation extends over all excited opposite parity states β. These states are derived from higher energy configurations than $4f^n$, such as $4f^{n-1}$5d (note figure 7). Since H_c is limited to terms with $n \leq 6$, this imposes a selection rule which tends to decrease the line intensity with increasing ΔJ up to $\Delta J = 6$.[10,11,12] This is one reason why the $4F_{3/2} \rightarrow 4I_{15/2}$ transition ($\Delta J = 6$) is approximately two orders of magnitude less intense than $^4F_{3/2} \rightarrow {}^4I_{11/2}$.

[12] JD Judd, Physical Review, 127, 760, 1962

[13] BC Wybourne, Journal of Chemistry and Physics, 72, 639, 1960

[14] IA Koningstein and JC Geusic, Physical Review, 136, A711, 1964
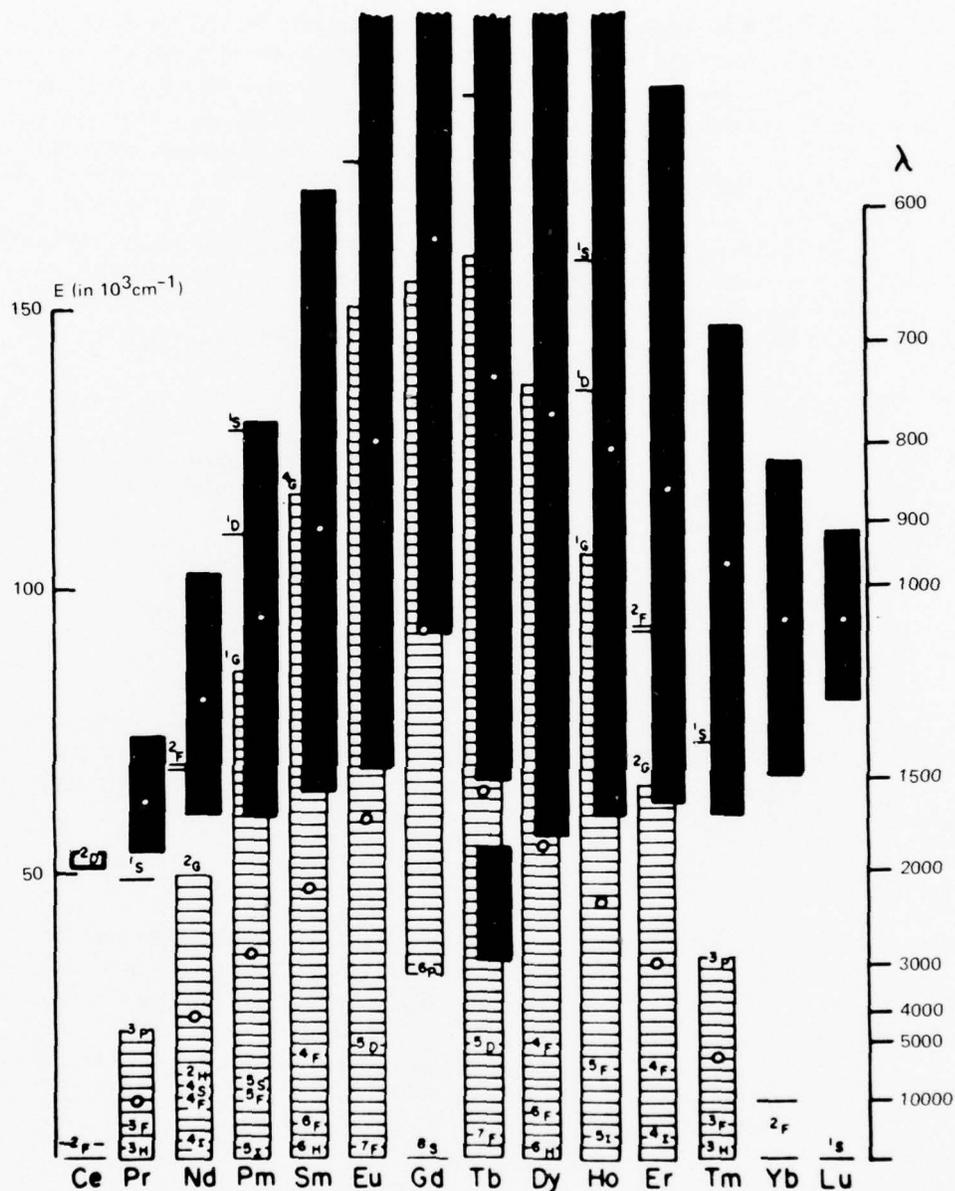
Figure 7. Energy level diagram of the 4f^n (white) and 4f^{n-1}5d (black) configuration of trivalent rare-earth ions.

Here again, while the perturbative treatment gives quantitative results, the group theor-etical approach is used to determine simple selection rules (this method only finds forbidden transitions, not allowed ones). Since the direct product of $\Gamma(|i>) \times \Gamma(|f>)$ when reduced in the site symmetry D_2 contains irreducible representations of the transition moment $\vec{r}$ (odd parity crystal terms arising from Y_3^{-2}, Y_5^{-2}, Y_5^{-4} spherical harmonics), no electric dipole transi-tions are forbidden (ie, no distinction, at least from group theory, as to π and σ electric dipole

16

radiation).[15,16] It is again only the very low site symmetry of D_2 that prevents selection rules; in general, different selection rules are obtained for transitions between states characterized by irreducible representations.

SINGLE PHONON INTERACTIONS

PHONONS IN YAG

Consider the system of a single rare-earth (RE) ion replacing an ion in a perfect crystal. The Hamiltonian for this system is

$$H = H_{el} + H_p + H_{ep} \tag{8}$$

where H_{el} is the electronic Hamiltonian of the RE ion in the perturbing crystal field of the other ions situated at their equilibrium positions:

$$H_{el} = H_{free\ ion} + H_c,$$

H_c is the crystal potential energy, H_p is the phonon Hamiltonian, and H_{ep} describes the interaction between the electronic state and the lattice phonons. The zero-order wave functions $| \psi >$, which are solutions of the equation

$$H_{el} | \psi > = E | \psi >,$$

are characterized by the free-ion quantum numbers ζLSJ, an irreducible representation of the RE ion site symmetry group G_s (ie, the point group symmetry in the vicinity of the RE ion), and a row of this representation (to specify each wave function within a degenerate representation).

Consider now the second two terms in H contained in equation (8). The phonon Hamiltonian H_p is invariant under the operation of the entire space group G. The vibrational wave functions are characterized by irreducible representations of this group. If a crystal has N unit cells and n ions per unit cell, we expect 3Nn possible modes of vibration. The size of the matrix to be diagonalized is reduced from a 3Nn $\times$ 3Nn matrix to a 3n $\times$ 3n matrix by considering translational symmetry; all possible values of k being contained within a Brillouin zone (BZ). There now remain 3n branches of the phonon spectrum to be obtained with each branch being defined by an irreducible representation of G. By convention, the 3n – 3 modes which do not have zero frequency at $\underline{k} = 0$ are called optical modes and those with $\omega(\underline{k} = 0) = 0$ are acoustical modes. It should be noted that the degeneracy of particular branches may be lifted along directions of lower symmetry of vector $\underline{k}$ than $\underline{k} = 0$. In the case of $Y_3 Al_2 (Al O_4)_3$, the space group is Ia 3d $(O_h)^{18}$, a body centered cubic Bravas lattice. There are 80 translationally invariant sites (n = 80) in YAG, and by reducing the reducible representation of ionic

[15] JC Prather, Atomic Energy Levels in Crystals, National Bureau of Standards Monograph 19, February 1961, US Government Printing Office, Washington, DC
[16] M Tinkham, Group Theory and Quantum Mechanics, McGraw-Hill Book Company, New York, 1964

displacements in each of the four types of sites (Y transforms like D_2, O like C_1 and the two types of Al sites like S_4 and S_6), the symmetry of all possible phonons at $\underline{k} \approx 0$ can be found (figure 8):

$$5A_{1u} + 3A_{1g} + 5A_{2u} + 5A_{2g} + 10E_u + 8E_g + 14T_{1g}$$

$$+18T_{1u} + 14T_{2g} + 16T_{2u}. \tag{9}$$

O_h	TYPICAL OPERATION	C_1 48 Q^{-2}	S_4 12 A1^{+3}	D_2 12 Y^{+3}	S_6 8 A1^{+3}
E	$\{\epsilon \mid 0\}$	144	36	36	24
$6\,C_4$	$\{\delta_{4z} \mid \tau(1)\}$	0	0	0	0
$3\,C_4^2$	$\{\delta_{2z} \mid \tau(2)\}$	0	-4	-4	0
$8\,C_3$	$\{\delta_{3xyz} \mid 0\}$	0	0	0	0
$6\,C_2$	$\{\delta_{2xy} \mid \tau(3)\}$	0	0	-4	0
I	$\{i \mid 0\}$	0	0	0	-24
$6\,S_4$	$\{i\,\delta_{4z} \mid \tau(1)\}$	0	-4	0	0
$3\,\sigma_h$	$\{i\,\delta_{2z} \mid \tau(2)\}$	0	0	0	0
$8\,S_6$	$\{i\,\delta_{3xyz} \mid 0\}$	0	0	0	0
$6\,\sigma_d$	$\{i\,\delta_{2xy} \mid \tau(3)\}$	0	0	0	0

δ_{3xyz} REPRESENTS A ROTATION OF $2/3\pi$ ABOUT [111]; δ_{2xy} REPRESENTS A ROTATION OF π ABOUT [110]; δ_{2z} AND δ_{4z} REPRESENT ROTATIONS OF π AND $\pi/2$ RESPECTIVELY ABOUT [001]; $\tau(1) = 1/4\,a\,(3, 1, 3)$; $\tau(2) = 1/2\,a\,(1, 0, 1)$; $\tau(3) = 1/4\,a\,(1, 1, 1)$.

Figure 8. The character table of the reducible representations generated by arbitrary displacements δ within YAG.

The above constitutes a total of 240 modes (ie, 3×80 branches of the $\omega(\underline{k})$ dispersion curve).

By assuming the harmonic approximation, the phonon Hamiltonian H_p becomes the sum of the harmonic-oscillator Hamiltonians for each normal coordinate:

$$H_p = \sum_{k\gamma r} \left[-\frac{1}{2}\,\hbar^2 \nabla^2_{Q_{k\gamma}^r} + \frac{1}{2}\,\omega^2_{k\gamma}\,Q^r_{k\gamma}\,Q^{*r}_{k\gamma} \right]. \tag{10}$$

The normal coordinate $Q_{k\gamma}^r$ is characterized by a wave $\underline{k}$, a small representation γ, and a row r of this representation (eg, to account for all polarizations within a T_{1g}, three-fold degenerate, vibration). The Schroedinger equation for a particular normal coordinate $Q_{k\gamma}^r$ is

$$\left[-\frac{1}{2}\,\hbar^2 \nabla^2_{Q_{k\gamma}^r} + \frac{1}{2}\,\omega^2_{k\gamma}\,Q^r_{k\gamma}\,Q^{*r}_{k\gamma} \right] \mid Q^r_{k\gamma}\,n_{k\gamma} > \tag{11}$$

$$= (n_{k\gamma} + \frac{1}{2})\,\hbar\,\omega_{k\gamma} \mid Q^r_{k\gamma}\,n_{k\gamma} >,$$

18

where $\omega_{k\gamma}$ and $n_{k\gamma}$ contain no subscript r since different rows within a representation indicate degeneracies. Therefore, the wave function of the whole system of phonons is the product

$$\prod_{k\gamma r} |\, Q_{k\gamma}^r \, n_{k\gamma}^r >$$
(12)

and the corresponding energy is

$$\sum_{k\gamma r} (n_{k\gamma} + \frac{1}{2}) \hbar \omega_{k\gamma}.$$
(13)

The three components of the displacement $x_i(n;\alpha)$, $i = 1, 2, 3$, of the αth ion in the nth unit cell are related to the normal coordinates by the linear transformation

$$x_i(n;\alpha) = \sum_{k\gamma r} (N m_\alpha)^{-1/2} C_{i\gamma r} (\vec{k};\alpha) \exp(i\,\vec{k}\cdot\vec{R}_n) Q_{k\gamma}^r \quad (12)$$

where $\vec{R}_n$ is the position of the nth unit cell and $C_{i\gamma\alpha}(\vec{k};\alpha)$ is a measure of how much a normal mode $Q_{k\gamma}^r$ affects the particular displacement $x_i(n;\alpha)$. In terms of boson operators,

$$Q_{k\gamma}^r = \sqrt{\frac{\hbar}{2\omega_{k\gamma}}} \left(a_{k\gamma r} + a_{-k\gamma r}^{\dagger} \cdot \right)$$

There are two orthonormality relations for the $C_{i\gamma r}$'s given by

$$\sum_{i\alpha} C_{i\gamma r}^* (\vec{k};\alpha) C_{i\gamma' r'} (\vec{k};\alpha) = \delta_{\gamma r, -\gamma' r'}$$

$$\sum_{\gamma r} C_{i\gamma r}^* (\vec{k};\alpha) C_{j\gamma r} (\vec{k};\alpha') = \delta_{ij} \delta_{\alpha\alpha'}.$$

Let V be the total interaction Hamiltonian between the RE ion and the rest of the ions in the crystal. It can be expanded in terms of the displacements $x_i(n;\alpha)$:

$$V = V_0 + \sum_{n\alpha i = 1, 2, 3} x_i(n;\alpha) \nabla_i (n;\alpha) V \,|_0 + \dots$$
(14)

The first term V_0 is the electrostatic (Stark) term which is incorporated in H_{el} as H_c. In the second term, the derivatives are evaluated at the equilibrium positions of all the ions, with the RE ion considered to be at the origin. By using equation (12) we can write the interaction Hamiltonian between the RE ion and the lattice vibration as

$$V_{ep} = \sum_{n\alpha i} x_i (n;\alpha) \nabla_i (n;\alpha) V \,|_0 = \sum_{k\gamma r} \left[\sum_{n\alpha i} (N m_\alpha)^{-1/2} C_{i\gamma r} (\vec{k};\alpha) \right.$$

$$\left. \exp(i\vec{k}\cdot\vec{R}_n) \nabla_i (n;\alpha) V \right] \cdot Q_{k\gamma}^r = \sum_{k\gamma r} V_{k\gamma}^{'\,r} Q_{k\gamma}^r.$$
(15)

19

The potential gradient terms $v'_{k\gamma}{}^{\Gamma}$ defined above operate only on the RE-ion electronic state while $Q_{k\gamma}{}^{\Gamma}$ (containing a and $a^{\dagger}$ terms) operate on phonon states only. This separation in V_{ep} is valid under the assumptions stated before, namely: $V_{ep} \ll V_c$ and $V_{ep} \ll V_{vib}$, ie, the mixing of electronic and vibrational states is small. Since we have assumed only a single RE ion interacting with the lattice phonons, this implies that V_{ep} is not invariant under the full space-group symmetry operations, but is invariant only under the operations of the ion-site symmetry G_s. Therefore, the phonon wave functions which transform according to the irreducible representations of G are combined into linear combinations which form a basis for the irreducible representation of G_s. In practice, this means that the representations arrived at by using the full space-group G are no longer irreducible in the less symmetric point group G_s and may be further reduced, analogous to splitting of residual degeneracy due to a lower symmetry distortion. If this is applied to the lattice normal coordinates $Q_{k\gamma}{}^{\Gamma}$, the following expression for V_{ep} is obtained:

$$V_{ep} = \sum_{k\Gamma r} v'_{k\Gamma}{}^{r} Q_{k\Gamma}{}^{r} . \tag{16}$$

The sum extends over all distinct stars of $\underline{k}$ in the BZ, over all irreducible representations Γ of G_s which appear in the reduction $G \to G_s$, and over all rows of the representation. The electronic operator $v'_{k\Gamma}{}^{r}$ now belongs to the same Γ as $Q_{k\Gamma}{}^{r}$ for a real representation and to Γ^* for a complex one. Knowing the transformation properties of the $v'_{k\Gamma}{}^{r}$'s will lead to the selection rules for phonon transitions (whether a phonon can interact with the RE ion).

For YAG, the reduction of the O_h representations in the site symmetry group D_2 results in the following:[15]

$$A_1 \to A$$
$$A_2 \to B_1$$
$$E \to A_1 + B_1$$
$$T_2 \to A_1 + B_3 + B_2$$
$$T_1 \to B_3 + B_2 + B_1 .^{[13]} \tag{17}$$

Thus, the 98 branches shown in Equation (9) become 240 non-degenerate vibrations:

$$28 A_g + 31 A_u + 27 B_{1g} + 33 B_{1u} + 28 B_{2g} + 34 B_{2u}$$
$$+ 28 B_{3g} + 34 B_{3u} \tag{18}$$

(the designation of parity above has no real meaning in a crystal without inversion symmetry and is left merely as a reminder of approximate parity).

NONRADIATIVE TRANSITION RATE

With the above specification of normal modes of the crystal, one can look at the quantum mechanics of a direct phonon transition. The transition probability per unit time is (implicitly averaging over direction and polarization of the phonons)

$$W_{i \to f} = \frac{2\pi}{\hbar} D(f) |<f|V_{ep}|i>|^2, \tag{19}$$

where $D(f)$ is the density of states defined such that $D(f) dE_f$ is the number of such states in the energy range dE_f. Under the assumption of a low mixing of vibrational and electronic wave functions, one can write the initial state

$$|i> = |\psi_i> \Pi_{k\Gamma r} |Q_{k\Gamma}^{r} n_{k\Gamma}> \tag{20}$$

and separate the matrix element into two parts. If we assume a phonon is absorbed and the electronic states go from $|\psi_i> \to |\psi_f>$, then we can write

$$|f> = |\psi_f> \Pi_{k\Gamma r}' |Q_{k\Gamma}^{r} n_{k\Gamma}> \times |Q_{k'\Gamma'}^{r'} (n_{k'\Gamma'} - 1)> \tag{21}$$

where the absorbed phonon in mode $Q_{k'\Gamma'}$ had an energy of $\hbar \omega_p' = H_{el} |f> - H_{el} |i>$. The matrix element $<f|V_{ep}|i>$ becomes

$$<f|V_{ep}|i> = \sum_{k\Gamma r} \Big\{ <\psi_f|v_{k\Gamma}^{'\ r}|\psi_i>$$

$$\left[\Pi_{k'\Gamma'r'}' |Q_{k'\Gamma'}^{r'} n_{k'\Gamma'}> \times |Q_{k''\Gamma''}^{r''} (n_{k''\Gamma''} - 1)> \right] *$$

$$\left(Q_{k\Gamma}^{r}\right) \left[\Pi_{k'\Gamma'r'} |Q_{k'\Gamma'}^{r'} n_{k'\Gamma'}> \right] \Big\}. \tag{22}$$

As indicated before, $Q_{k\Gamma}^{r}$ can be written in terms of boson annihilation-creation operators as

$$Q_{k\Gamma}^{r} = \left(\frac{\hbar}{2\omega_{k\Gamma}}\right)^{1/2} (a_{k\Gamma r} + a_{-k\Gamma r}^{\dagger}). \tag{23}$$

so that equation (22) can be reduced to (from orthogonalization)

$$<f|V_{ep}|i> = <\psi_f|v_{k\Gamma}^{'\ r}|\psi_i> \left(\frac{\hbar n_{k\Gamma}}{2 \omega_{k\Gamma}}\right)^{1/2} \tag{24}$$

(omitting the primes on k, Γ, and r). The transition probability per unit time becomes,

$$W_{i \to f} = \pi D(Q_{k\Gamma}) \frac{n(\omega_{k\Gamma})}{\omega_{k\Gamma}} |<\psi_f|v_{k\Gamma}^{'\ r}|\psi_i>|^2. \tag{25}$$

The motivation for obtaining exact normal modes and for determining precisely the transformation characteristics for the $v_{k\Gamma}'^{\ r}$'s is now clear. If the direct product of the irreducible representation for ψ_f and ψ_i does not contain the irreducible representation of $v_{k\Gamma}'^{\ r}$ (hence, the irreducible representation of $Q_{k\Gamma}^{r}$ in the point group G_s) then the transition is not allowed. Thus, by knowing the transformation properties of the initial and final electronic wave functions, and the transformation properties of the normal modes of vibration, one can, via group theory, determine whether a particular phonon can interact with the RE ion; eg, whether it can cause broadening.

With the case of Nd^{+3} in low symmetry YAG, the formal approach proves disconcerting. In the D_2 point group symmetry of the Y site, it was determined that all electronic wave functions transform as E-type irreducible representations. Thus, one must reduce $E \times E$ in D_2, which yields, recalling figure 4,

$$E \times E = A + B_3 + B_2 + B_1.^{[17]} \tag{26}$$

So, for the low site symmetry of D_2, it is clear from equation (26) that <u>all</u> 240 nondegenerate modes may couple to the Nd^{+3} ion and, in theory, all 240 may stimulate nonradiative decays. Group theory does not specify the magnitude of the interaction, however. Obviously, the approximate odd parity modes will, in general, have smaller values for $< f \mid v'_{k\Gamma}{}^r \mid i >$ than

modes with approximately even parity. Also, the nearest neighbors of the Nd^{+3} ion will interact the most, ie, the $v'_{k\Gamma}{}^r$ are different for various normal modes. With the formalism well

established, one may begin to analyze the specific example of Nd^{+3} in YAG using various degrees of approximation.

INTERNAL PHONONS

First, it is expedient to assume that the lowest order interactions are those with the eight nearest neighbor oxygen ions. The XY_8 type molecule is assumed isolated from the lattice in that the molecule has its own set of normal modes of vibration. With ionic radii for 0^{-2}, Nd^{+3}, Y^{+3}, and Al^{+3} being 1.40 Å, 1.23 Å, 0.93 Å and 0.50 Å respectively,[19] this is easy to accept. What is planned is to consider the eight 0^{-2} ions coordinated around the Nd^{+3} ion to be in cubic 0_h symmetry, find the modes of vibration of this isolated complex and then reduce the internal modes of vibration in D_2 symmetry; retaining the approximate state of parity.

These internal normal modes of vibration are not lattice waves, though. The Q's arrived at in equation (25) will stimulate the localized modes to oscillate and the localized modes will affect the transition (in our approximation). Thus, if $\hat{Q}_K$ is the Kth normal mode of the molecular complex, one can write the electron-phonon interaction as

$$V_{ep} \cong \sum_K \hat{v}'_K \ \hat{Q}_K. \tag{27}$$

where the approximation symbol is intended as a reminder that only nearest neighbors are interacting and that we have assumed the XY_8 type molecule to be isolated. Since the lattice vibrations are complete, the internal normal mode $\hat{Q}_K$ can be expanded linearly in terms of lattice vibrations:

$$\hat{Q}_K = \sum_{k\Gamma r} a_{K, k\Gamma r} Q_{k\Gamma}{}^r.$$

where the $a_{K, k\Gamma r}$'s are the mixing factors. This results in a minor complication of equation (24), in that the lattice normal modes must mix to give an internal mode; one no longer has the simple orthogonalization. The result is

$$W_{i \to f} = \pi \, D(\omega_{k\Gamma}) \, \frac{n(\omega_{k\Gamma})}{\omega_{k\Gamma}} \, | \, \sum_K a_{K, k\Gamma r} < \psi_f \, | \, \hat{v}'_K \, | \, \psi_i > |^2. \qquad (28)$$

The above expression, for the transition rate of the direct-phonon absorption, can be interpreted as follows: A lattice phonon in mode $k\Gamma r$, and energy $\hbar\omega_{k\Gamma}$, interacts with the molecular complex XY_8. This causes displacement of the nearest neighbors to the RE ion which have been described in terms of internal normal modes of the complex (the amount of interaction being given in terms of the $a_{K, k\Gamma r}$ coefficients). This variation in the crystalline field induces the transition of the electronic state and the annihilation of a phonon in mode $k\Gamma r$.

The mixing coefficients $a_{K, k\Gamma r}$ will thus become very mode- (ie, frequency) dependent. Not only will $D(\omega_{K\Gamma})$ and $n(\omega_{k\Gamma})$ measure how many phonons are present to induce transitions, but the a's will measure how much those particular lattice vibrations affect the nearest neighbors of the RE ion, while the $\hat{v}'_K$'s determine how much the nearest neighbors affect the RE ion (induce transitions). Therefore, the a coefficients conceal peaks in the $W(\omega)$ curve: a large peak is expected whenever a lattice phonon highly couples into the internal mode (and this is when the a coefficient, and thus the $\hat{Q}_K$ is large). This is another reason for the concern over internal modes. Besides requiring the transformation properties of $\hat{Q}_K$ to find phonon selection rules, the number of possible internal modes affecting the RE ion will be an indication of the complexity of the $W(\omega)$ curve.

Even more concealed is the added frequency dependence in $W(\omega)$ due to the potential gradient term $\hat{v}'_K$. The origin of this dependence is seen if one recalls that the Stark splitting of each J manifold arises from matrix elements of the crystalline potential energy H_c. Since the coefficients of H_c determine the Stark splitting, and the amount of splitting determines the phonon frequency ω, there is a relation between H_c (and thus the derivatives $\hat{v}'_K$) and ω. A generalization about the frequency dependence of $< \psi_f | \hat{v}'_K | \psi_i >$ is very difficult.

The first step in this nearest-neighbor solution is to find the modes of vibration of this isolated XY_8 molecular-like system.[17] The nine ions have a total of 27 degrees of freedom and, by reducing the reducible representation of ionic displacements in the O_h point group, we find the following symmetries:[1,16]

$$A_{1g} + E_g + T_{1g} + 2T_{2g} + A_{2u} + E_u + 3T_{1u} + T_{2u}. \qquad (29)$$

If one T_{1u} and one T_{1g} representation is removed to account for translational and rotational degrees of freedom, the internal, localized modes remain:

$$A_{1g} + E_g + 2T_{2g} + 2A_{2u} + E_u + 2T_{1u} + T_{2u}. \qquad (30)$$

In a similar manner by which equation (15) was derived, the above representations can be reduced in the actual point group D_2. The irreducible representations of O_h reduced in the manner shown in equation 17 so that the following internal modes are possible:

$$4A_g + B_{1g} + 2B_{2g} + 2B_{3g} + 3A_u + B_{1u} + 3B_{2u} + 3B_{3u}. \qquad (31)$$

---

[17] JH Van Vleck, Journal of Chemistry and Physics, 7, 72, 1939

The distinction with respect to parity is used only as an approximation (formally we can say that we are reducing in the D_{2h} group and consider the D_2 site symmetry as a slight distortion to D_{2h}). Thus, there are 21 possible vibrations of the XY_8 complex; 9 even and 12 odd. So in the matrix elements of $<\psi_f \mid \hat{v}'_K \mid \psi_i>$, one may expect 9 large values corresponding to the 9 approximately even parity nondegenerate modes.

RAMAN-LIKE INTERACTIONS

The formal derivation of the direct-phonon transition rate illustrates the complexities which result in a crystal of low-site symmetry. This detailed derivation will not be followed in the even more complicated derivation of the Raman broadening term. This is done for two reasons. First, the inherent formalism of a second-order process introduces complications which obscure the desired result by requiring the determination of parameters impossible to measure and extremely difficult to calculate. Second, a formal derivation of the Raman broadening mechanism is not necessary to determine the parameters in which we are interested. In the final conclusion we will have to rely upon experiment anyway to normalize the result and this implicitly calculates all matrix elements and makes all the necessary summations.

Just as in the direct process, we desire to find a transition rate; this time for the two-phonon process exchanging states between two energy levels of a single RE ion situated in a perfect crystal. Schematically, we have the situation shown in figure 9. For an upward transition, a phonon of frequency ω_1 is absorbed and a phonon of frequency ω_2 is emitted. Since the transition occurs very fast (via the virtual intermediate state), Heisenberg broadening results. As before, the transition is described by an interaction Hamiltonian; which means we must expand the crystalline potential as seen by the RE ion in displacements of the surrounding ions, this time to second order.
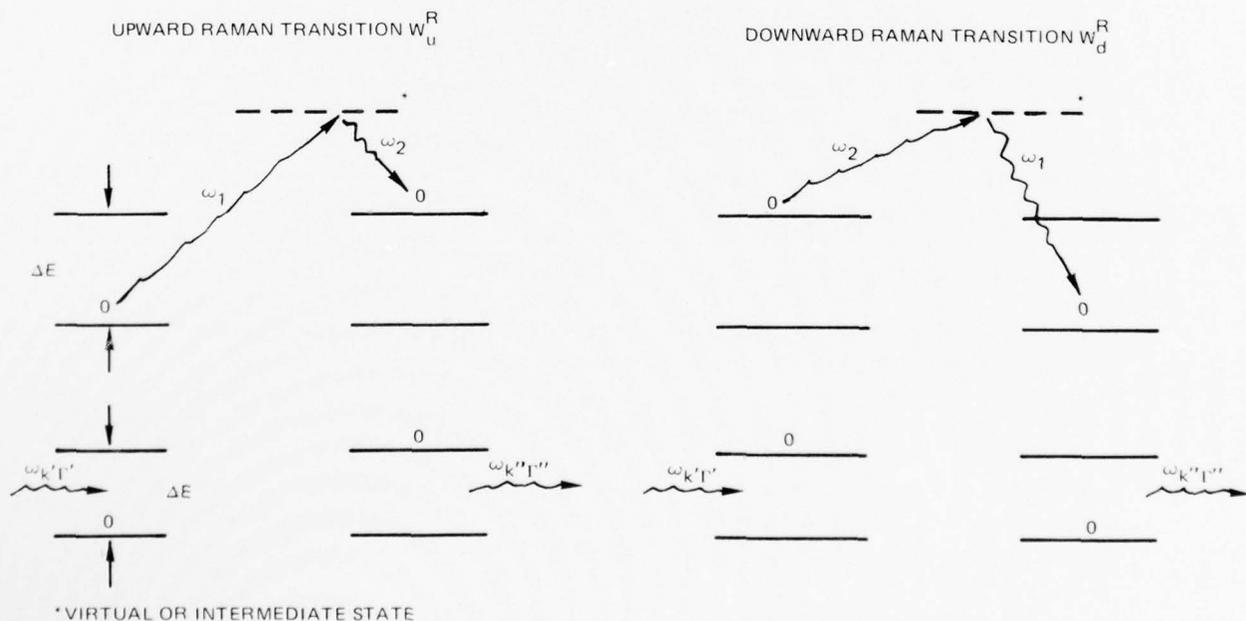

Figure 9. Two schematic representations of the upward and downward Raman non-radiative energy level exchange mechanisms.

24

$$V_{ep} = V_0 + V_{ep}^{(1)} + V_{ep}^{(2)} + \ldots \tag{32}$$

V_0 is still the static Stark term and $V_{ep}^{(1)}$ is the first-order term used to calculate W^D (direct),

$$V_{ep}^{(1)} = \sum_{n\,\alpha\,i = 1,\,2,\,3} x_i\,(n;\alpha)\,\Delta_i\,(n;\alpha)\,V\mid_0, \tag{33}$$

where $x_i\,(n;\alpha)$ is the ith *direction of the displacement of the* α^{th} *ion in the* n^{th} *unit cell.* $\Delta_i\,(n;\alpha)V$ is the ith component of the derivative of V taken at the αth ion of the nth unit cell and it is evaluated at the RE ion (since this is where the effect happens). The second-order expression for $V_{ep}^{(2)}$ is

$$V_{ep}^{(2)} = \frac{1}{2} \sum_{n\alpha i} \sum_{\underline{n\alpha i}} \left\{ x_i\,(n;\alpha)\,x_{\underline{i}}\,(\underline{n;\alpha})\,[\,\nabla_i\,(n;\alpha)\,\nabla_{\underline{i}}\,(\underline{n;\alpha})]\,V \right\} \mid_0, \tag{34}$$

where the last expression is the two-component derivative of V, namely

$$\frac{\partial^2 V}{\partial x_i\,(n;\alpha)\,\partial x_{\underline{i}}\,(\underline{n;\alpha})}\,.$$

Therefore, in the same way equation (14) was derived, we can write $V_{ep}^{(2)}$ as

$$V_{ep}^{(2)} = \sum_{k\gamma r} \sum_{\underline{k\gamma r}} \left[\tilde{v}_{k\gamma;\underline{k\gamma}}^{\,r\,\underline{r}}\; Q_{k\gamma}^{\,r}\; Q_{\underline{k\gamma}}^{\,\underline{r}} \right], \tag{35}$$

where

$$\tilde{v}_{k\gamma;\underline{k\gamma}}^{\,r\,\underline{r}} = \frac{1}{2} \sum_{n\alpha i} \sum_{\underline{n\alpha i}} \left[(Nm_\alpha)^{-1}\,C_{i\gamma r}\,(\vec{k};\alpha) \right.$$

$$\left. C_{\underline{i\gamma r}}\,(\vec{k};\alpha)\exp(i\,\vec{k}\cdot(\vec{R}_n + \vec{R}_{\underline{n}}))\,\nabla_i\,(n;\alpha)\nabla_{\underline{i}}\,(\underline{n;\alpha})V\mid_0 \right]. \tag{36}$$

Again, $\vec{R}_n$ is the position of the nth unit cell and the $C_{i\gamma r}\,(\vec{k};\alpha)$ coefficients measure how much a normal mode $Q_{k\gamma}^{\,r}$ affects the particular displacement $x_i\,(n;\alpha)$.

Therefore, we may get Raman-like transitions two ways: first order in $V_{ep}^{(2)}$ or second order $V_{ep}^{(1)}$. It is here that the formalism becomes cumbersome and it is here that the derivation will be streamlined. From equation (18) we have (neglecting multiplicative constant)

$$W^R \propto |<f\mid V_{ep}^{(2)}\mid i>|^2\,D(\nu).$$

25

Here $D(\nu)$ is the <u>total</u> density of final states. For an upward Raman transition we expect initial and final states which look like

$$|i> = | \psi_i > \Pi_{k\Gamma r} | Q_{k\Gamma}^{\Gamma} \; n_{k\Gamma} > \qquad (37)$$

$$|f> = | \psi_f > \Pi'_{k\Gamma r} | Q_{k\Gamma}^{\Gamma} \; n_{k\Gamma} > | Q_{k'\Gamma'}^{\Gamma'} \; (n_{k'\Gamma'} - 1) > | Q_{k''\Gamma''}^{\Gamma''} \; (n_{k''\Gamma''} + 1) >$$

for the process shown in figure 9. When the $Q_{k\Gamma}^{\Gamma}$'s are written in terms of boson annihilation-creation operators, we get terms like

$$a_{k''\Gamma''r''} \cdot a_{k'\Gamma'r'}^{\dagger}$$

which "connect" $|i>$ and $|f>$. Therefore, Raman transition rates are derived which look like

$$W_u^R \propto \frac{n(\omega_{k\Gamma}) \, [n(\omega_{k'\Gamma'}) + 1]}{\omega_{k\Gamma} \, \omega_{k'\Gamma'}} \; | < \psi_i | \tilde{v}_{k\Gamma \, ; \, k'\Gamma'}^{r \, r'} | \psi_f > |^2 \; D(Q_{k\Gamma}) \, D(Q_{k'\Gamma'}), \quad (38)$$

rearranging primes.

As stated earlier, the purpose of this calculation is to find the temperature dependence of the linewidth. In order to accomplish this rigorously, one must go through the same internal-model analysis as that done for W^D. As will be shown later, the nature of the crystal reduces the practicality of carrying out such calculations. Instead, a simple approximation is to be used to obtain a good fit to the experimental curve, with enough versatility retained in the formalism to allow prediction of other ion-host combinations. As was emphasized in the direct case, the detailed structure of the $D(\omega)$ curve tends to smooth out when sums are taken and the real density of states is used and especially if lattice anharmonicity is considered. In the Raman case, the integration over all phonon modes inducing transitions will introduce even more smoothing. For this reason we can consider the Raman transition rate as simply

$$W_u^R = C \, n(\omega_1) \, [n(\omega_2) + 1] \, D(\omega_1) \, D(\omega_2)$$

$$W_d^R = C \, [n(\omega_1 + 1)] \, n(\omega_2) \, D(\omega_1) \, D(\omega_2), \qquad (39)$$

where in equilibrium $W_u = W_d \, e^{-\Delta E/kT}$. C is a single multiplicative parameter taking into account all matrix elements, summations, internal mode mixing, and the like. In practice, this will be determined experimentally by normalizing the linewidth to experimental results at one temperature.

The use of $V_{ep}^{(1)}$ in second order results in a similar expression (with different matrix elements). Here we use

$$W^R \propto \sum_m \sum_{k\Gamma r} \sum_{k'\Gamma'r'} \frac{| < f | V_{ep}^{(1)} | m > < m | V_{ep}'^{(1)} | i > |^2}{(E_m - E_i)} \, D(E_f - E_i) \qquad (40)$$

26

where m is a member of the complete set of wave functions comprising the intermediate states. Since the difference between this expression and the one used in first order only changes C in equation (39), we will still use (39) as the expression for the Raman transition rate.

INTERACTING PHONONS

INTERNAL MODES

In order to find the thermal dependence of linewidth, the spectrum of those phonons affecting the active ion must be determined. As was shown, the existence of a lattice phonon is not a guarantee it will couple into and affect the active ion, inducing a non-radiative transition. Acoustic phonons have high densities of states and large occupation numbers, yet they correspond to movement of the entire unit cell and, therefore, small relative motion to the active ion to induce transitions. The determination of a tractable model for interacting phonons is what is sought in this section. If the range of strongly interacting internal modes is determined, the predominant broadening mechanism can be found (whether direct or Raman), the transition rate can be summed for all effective modes, and a simple, compact linewidth formalism can be found. The degree of experimental fit of the final linewidth theory will justify the approximations made.

The Debye theory for acoustic phonons, when applied to the system of a rare-earth impurity ion located in a simple crystal, results in a linewidth theory well illustrated in articles such as Yen, Scott and Schawlow.[2] This approximation allows all lattice phonons to couple into the active ion, gives no clues as to which broadening mechanisms predominate and results in non-analytical solutions. In addition, use of the Debye theory requires many curve fitting parameters to fit experimental data, both a multiplicative parameter as well as a special Debye cut-off frequency (unrelated to simple bulk thermodynamic quantities) for each set of levels. This theory then does not predict the functional dependence of linewidth with temperature, it merely can be made to fit the experiment. This is often at the expense of absurd implications with respect to physical parameters such as bulk modulus, thermal conductivity, heat capacity, and the like.[18] As will be shown later, only the insensitivity of the thermal dependence of linewidth with the structure of the density of states accounts for the success in fitting the theoretical model to the experimental results.

Let us look at another approach to the linewidth problem, employing localized modes. Consider again the results of equation (25) employing internal modes in the single phonon case. Here all have three parameters, $D(\omega_{k\Gamma})$, $a_{K, k\Gamma r}$ and $< \psi_f | \hat{v}_{K'} | \psi_i >$ – all of which measure the effect of a lattice phonon of frequency $\omega_{k\Gamma}$ on the active ion. Recall that $D(\omega_{k\Gamma})$ is the density of states of the lattice phonon of frequency $\omega_{k\Gamma}$, $a_{K, k\Gamma r}$ is a measure of how much the lattice phonon affects the localized mode K, and $\hat{v}_{K'}$ determines how much the internal mode affects the RE ion and induces nonradiative transitions). Here, for simplicity, all three parameters are combined and called the effective density of states. We have merely

$$W_d^D = D'(\omega)(n(\omega) + 1)$$

$$W_u^D = D'(\omega) n(\omega).$$

with similar results for the Raman case (equation (39)). $D'(\omega)$ is the spectrum of the effective internal phonons and is an average over <u>all</u> lattice phonons reflecting how the lattice phonons at frequency ω affect the rare-earth ion. Now the non-radiative transition rate is sensitive to only these active internal modes rather than all lattice phonons.

What does $D'(\omega)$ look like? Certainly it will not be a continuum like the Debye theory. In first order, it will most closely resemble the Einstein theory, discrete normal frequencies for each internal normal mode coupling into the active ion. Figure 10 illustrates the difference. Fundamentally, the continuum described by the Debye theory is replaced by a spectrum reflecting the active internal normal modes; exhibiting a minimum as well as a maximum frequency of vibration of the RE ion, nearest-neighbor complex. This will have immediate impact on the direct phonon transition rate, as low frequency phonons resonant with energy level separations may not exist in $D'(\omega)$. One can also predict that there is width to the lines in $D'(\omega)$ due primarily to anharmonic effects which will cause overlap of peaks. Therefore, all that is to be determined to find linewidth thermal variations are the frequencies of the normal modes and the relative magnitude. As will be seen later, more important than the precise values of the vibration frequencies will be the range of active interacting phonons in $D'(\omega)$. With $D'(\omega)$ modeled, the thermal variations of the linewidth can be solved, in this case, analytically.
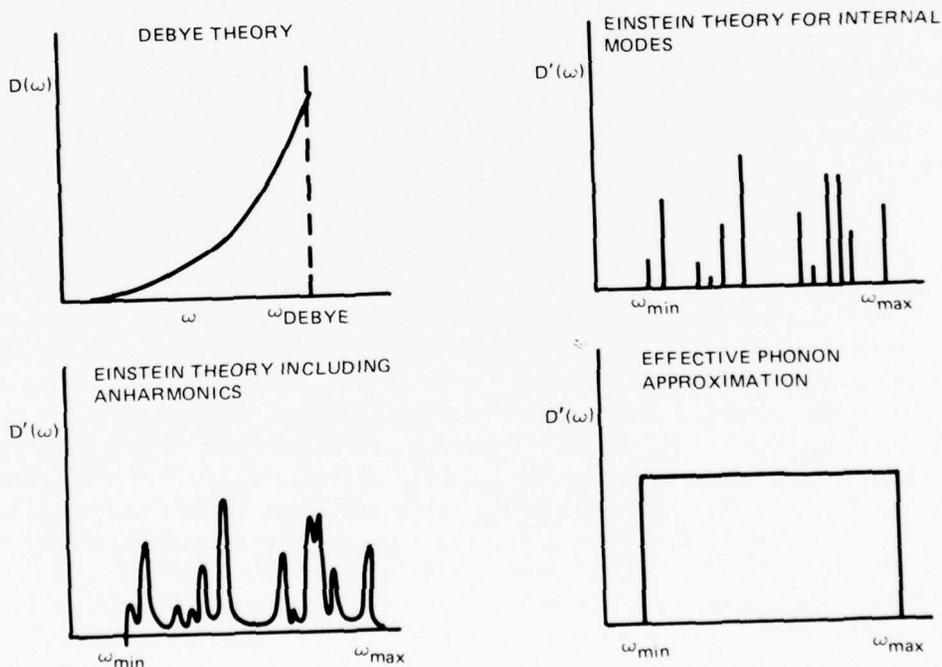

Figure 10. Four models for the density of lattice and internal phonons.

[18] T Kushida, Physical Review, 185, 500, 1969

VIBRONIC TRANSITIONS

One method of obtaining insights as to the structure of the effective phonon spectra *is to look at the vibrational sidebands* accompanying the electric dipole transitions in RE-doped crystals. Since direct vibrational data are difficult or impossible to obtain, this is extremely valuable. Here the vibronic data will reflect the range of interacting modes affecting the impurity RE ion and will establish the degree to which these modes are indeed "internal." By examining the structure and number of phonon-assisted sidebands, and by recognizing that vibronics are also a nearest-neighbor phenomena, one should be able to establish, at least, the frequencies of the internal highly coupled modes in the crystal. Since these data are usually taken at low temperatures and with high dopant impurity concentrations to facilitate the experiment, the application of these results to the nonradiative energy-level exchange problem will not give the exact shape of $D'(\omega)$.

Let us find a simple expression for *the intensity of the vibronic emission or absorption*. As before, for the static lattice transition in a crystal with inversion symmetry, electric-dipole transitions are allowed only if there is an odd parity component of the interaction Hamiltonian to admix opposite parity states. The odd parity lattice vibrations will now cause the admixing. Consider the electric-dipole transition matrix element

$$< \psi_u | -e\, \vec{r} | \psi_g >$$

between the upper state $| \psi_u >$ and the lower state $| \psi_g >$. If no perturbation of these states exist, the matrix element will be zero since both levels are derived from the same $4f^n$ configuration and have the same parity. The application of the electron-phonon interaction Hamiltonian V_{ep} to the wave functions will cause admixing with excited opposite-parity wave functions from the $4f^{n-1}5d$ configuration, say, and permit transitions. Consider the unperturbed upper state

$$| \psi_u > \Pi_{k\Gamma r} | Q_{k\Gamma}^r n_{k\Gamma}^r >.$$

Since we know that V_{ep} in first order cannot connect states separated by more than one quantum number, we can write the perturbed upper state — containing the admixed state $| \psi_\beta >$ *due to one phonon*

$$| \chi_u > = | \psi_u > \Pi_{k\Gamma r} | Q_{k\Gamma}^r n_{k\Gamma} > +$$

$$- \Sigma_\beta \{ [| \psi_\beta > \Pi'_{k\Gamma r} | Q_{k\Gamma}^r n_{k\Gamma} > | Q_{k'\Gamma'}^{r'} n_{k'\Gamma'} - 1>] * V_{ep}$$

$$\frac{[| \psi_u > \Pi_{k\Gamma r} | Q_{k\Gamma}^r n_{k\Gamma} >]}{E_\beta - E_u} | \psi_\beta > \Pi'_{k\Gamma}^r | Q_{k\Gamma}^r n_{k\Gamma} > | Q_{k'\Gamma'}^{r'} n_{k'\Gamma'} - 1 > \}$$

$$- \Sigma_\beta \{ [| \psi_\beta > \Pi'_{k\Gamma r} | Q_{k\Gamma}^r n_{k\Gamma} > | Q_{k'\Gamma'}^{r'} n_{k'\Gamma'} + 1 >] * V_{ep}$$

$$\frac{[| \psi_u > \Pi_{k\Gamma r} | Q_{k\Gamma}^r n_{k\Gamma} >]}{E_\beta - E_u} | \psi_\beta > \Pi'_{k\Gamma r} | Q_{k\Gamma}^r n_{k\Gamma} > | Q_{k'\Gamma'}^{r'} (n_{k'\Gamma'} + 1) > \}. \quad (41)$$

Here, $|\psi_u\rangle$ and $|\psi_g\rangle$ are purely electronic wave functions with the sum β extending over all excited, opposite-parity electronic states. Again, the lower state becomes

$$|\chi_g\rangle = |\psi_g\rangle \Pi'_{k\Gamma r} |Q^r_{k\Gamma} \; n_{k\Gamma}\rangle \, |Q^{r'}_{k'\Gamma'} \, (n_{k'\Gamma'} - 1)\rangle$$

$$- \Sigma_\beta \{[\, |\psi_\beta\rangle \Pi_{k\Gamma r} |Q^r_{k\Gamma} \; n_{k\Gamma}\rangle]^* \, V_{ep}$$

$$\frac{[\,|\psi_g\rangle \Pi'_{k\Gamma r} |Q^r_{k\Gamma} \; n_{k\Gamma}\rangle |Q^{r'}_{k'\Gamma'} \, (n_{k'\Gamma'} - 1)\rangle]}{E_\beta - E_g} \, |\psi_\beta\rangle \Pi_{k\Gamma r} |Q^r_{k\Gamma} n_{k\Gamma}\rangle \quad . \quad (42)$$

Here a simplification is made. Since most vibronic data are taken at low temperatures (to avoid second order effects such as anharmonics) the limit of $T = 0°K$ is assumed. Thus, the occupation numbers for all modes tend to zero. Therefore, using the first order expression for V_{ep} given in equation (14), orthogonalization of the wave functions, and retaining only first order terms, we obtain

$$\langle \chi_u | - e\,\vec{r} | \chi_g \rangle =$$

$$\Sigma_\beta \, \frac{\langle \psi_\beta | v'^r_{k\Gamma} | \psi_g \rangle \langle \psi_u | - e\,\vec{r} | \psi_\beta \rangle}{E_\beta - E_g} \left(\frac{\hbar}{2\omega_{k\Gamma}}\right)^{1/2}$$

$$-\Sigma_\beta \, \frac{\langle \psi_\beta | v'^r_{k\Gamma} | \psi_u \rangle \langle \psi_\beta | - e\,\vec{r} | \psi_g \rangle}{E_\beta - E_u} \left(\frac{\hbar}{2\omega_{k\Gamma}}\right)^{1/2} \quad . \qquad (43)$$

This corresponds to a transition of the RE ion from state g to state u plus the creation of one phonon in mode (kΓr). Here we see that $|\psi_\beta\rangle$ must indeed be derived from an opposite parity configuration to remain non-zero.

The transition probability per unit time is given by the familiar relation

$$W = \left(\frac{2\pi}{\hbar}\right) \langle \chi_u | - e\,\vec{r} | \chi_g \rangle \, \rho(E) \, .$$

where $\rho(E)$ is the density of final states composed of the product of the lattice phonon density of states $D(\omega)$ and the electronic states $g(E - \hbar)$. Since the energy spread of the electronic states is much smaller than the range of the phonon states, $g(E - \hbar\omega) = \delta(E - \hbar\omega - \omega_{k\Gamma})$ and the vibronic spectrum reflects the structure of $D(\omega)$ (figure 11). The precise structure of $D(\omega)$ is difficult to determine, though, because of the electronic matrix elements in equation (43) and because of the difference in the matrix elements involving $v^r_{k\Gamma}$. For example, since the ψ_β is opposite parity to ψ_u and ψ_g, only the odd parity vibrations can have non-zero matrix elements. Recall that the expression for the single phonon nonradiative transition depends on the even parity normal modes. The group theoretical selection rules are also similar to those for phonon nonradiative transitions. This states that
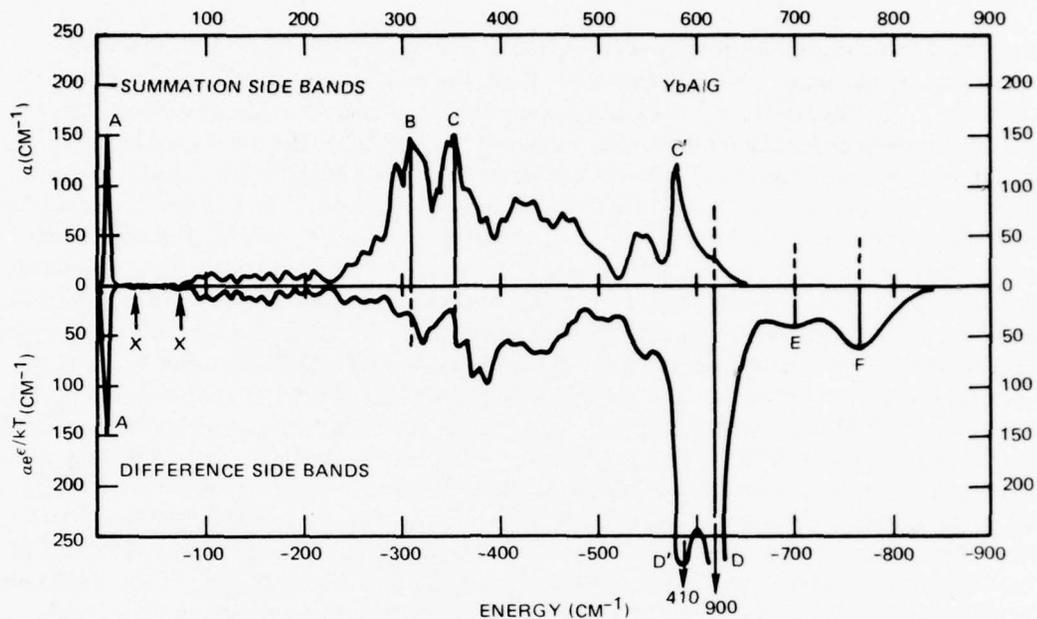
Figure 11. Vibronic spectra at low temperatures for $Yb_3 Al_2 (AlO_4)_3$ indicating effective phonons.[15]

$$\langle \chi_u | - e \vec{r} | \chi_g \rangle = 0$$

if

$$\Gamma_u^* \times \Gamma_g \times \Gamma_{Q_{k\Gamma}^r}$$

does not contain an irreducible representation of the transition moment $\vec{r}$ when reduced in the site symmetry G_s (where Γ_u and Γ_g are the irreducible representations of the upper and ground states respectively, and $\Gamma_{Q_{k\Gamma}^r}$ is the irreducible representation of the normal mode $Q_{k\Gamma}^r$ of G_s). In crystals such as YAG, which do not contain inversion symmetry, parity is not a good quantum number and normal modes are composed of both even and odd parity parts. Also, the low D_2 site symmetry does not exclude any transitions due to the selection rules and all modes can cause sidebands. What is significant is that now the range of interacting phonons can be determined by examining the vibronic spectra. By counting the number of sidebands and comparing this to the number predicted from the internal-mode approximation, the degree of isolation of the internal modes can also be investigated.

PRESUMED INTERACTING EFFECTIVE MODES

In order to find the effective phonons of the system of Nd^{+3} in YAG, the vibronic spectra at low temperatures can be examined. The data available[19] are for $Yb_3 Al_2 (AlO_4)_3$.

---

[19] RA Buchanan, Physical Review, 159, 345, 1967

Since the difference in atomic weight between Y_b^{+3} and Nd^{+3} is 173 vs 144, this data is assumed to be adequate, though not precise. Also, Buchanan states that using Yb Al G instead of Y^{+3} doped YAG results in larger absorption coefficients without seriously perturbing the symmetries and so facilitates the experiment. The results are shown in figure 11. Here we find approximately 20 large sidebands occurring between 250 cm^{-1} and 570 cm^{-1} and a small group of approximately nine smaller ones from 75 cm^{-1} to 225 cm^{-1}. Recalling the results of the group theoretical reduction of the XY_8 complex, we expect the internal normal modes to consist of nine approximately even-parity and 12 approximately odd-parity vibrations, a total of 21 close-coupled modes corresponding to the XY_8 molecular system of Nd^{+3} and 0^{-2}. The conventional normal-mode analysis of the 80 ions in the unit cell predicts 240 possible modes seen by the Nd^{+3} ion in D_2 site symmetry. The data using Yb Al G fit well with the predicted results. The range of internal vibrations then, is confined to a region approximately 300 cm^{-1} wide containing narrow peaks corresponding to highly coupled modes (contrasting sharply with the Debye prediction). The small peaks on the low frequency side are thought to be next nearest-neighbor interactions of low energy between the RE ion and the Al^{+3} ion. Since the atomic weight of Al is 27 and that for 0^{-2} is 16, we should expect a lower vibration spectrum. Also, the larger inter-atomic spacing to the Al^{+3} ion will result in lower frequency modes as well as smaller coupling (as seen by the amplitude of the sidebands). Therefore, let us choose to model the complicated effective phonon spectrum by a simple uniform density of modes ranging from approximately 250 cm^{-1} to 570 cm^{-1} (note figure 12):

$$D(\omega) = \begin{cases} \bar{D} & 250 \text{ cm}^{-1} < \hbar\omega < 570 \text{ cm}^{-1} \\ 0 & \text{otherwise} \end{cases} \tag{44}$$
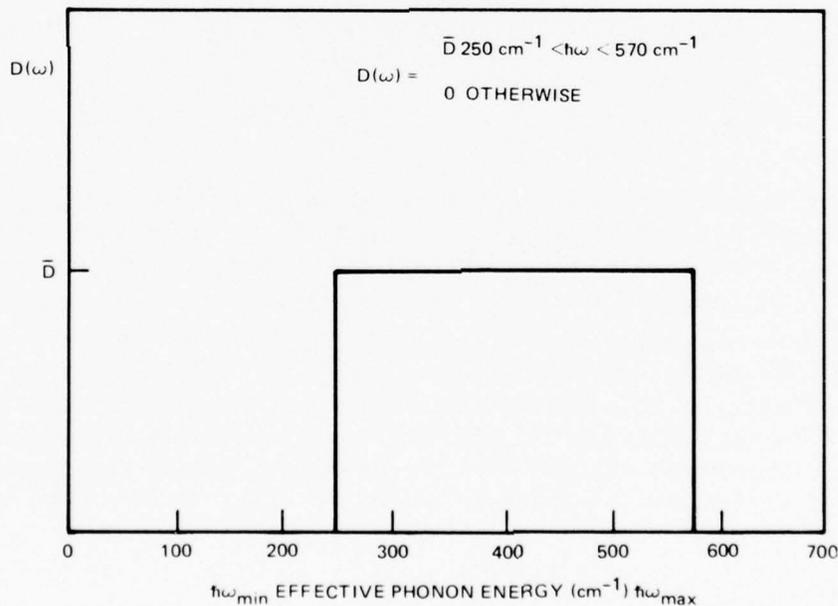

Figure 12. Uniform density model for the effective modes in Nd^{+3} YAG.

32

(with $\bar{D}$ a constant). Since incorporation of the precise shape (if it could be extracted from the data available) would result in another numerical result, let us try the above approximation and examine the quality of fit to the experiment. After the next section we will examine the prediction of thermal, linewidth variation incorporating the above approximation.

DEBYE LINEWIDTH THEORY

What is presented in this section is a brief overview of the Debye theory for the thermal dependence of linewidth, best presented by Yen, Scott and Schawlow.[2] This is done primarily to place in proper perspective the theory to be presented. Also, this furnishes a theoretical base to the effective-mode theory to be presented later. Assuming a completely Debye model for the crystal, Yen, et al, begin by writing the Hamiltonian of the impurity ion in a host crystal as

$$H_{tot} = H_0 + H_p + H_1 ,$$

where H_0 describes the ion in the presence of a crystalline field, H_p describes the phonon system

$$H_p = \Sigma_k (a_k^\dagger a_k + \frac{1}{2} \hbar \omega_k) ,$$

and H_1 describes the interactions between the ion and the lattice vibrations

$$H_1 = \Sigma_k \left(\frac{\hbar}{2Mv^2}\right)^{1/2} C \omega_k^{1/2} (a_k - a_k^\dagger) +$$

$$\Sigma_{k,k'} \left(\frac{\hbar}{2Mv^2}\right) D \omega_k^{1/2} \omega_{k'}^{1/2} (a_k - a_k^\dagger)(a_{k'} - a_{k'}^\dagger) + \ldots$$

$$= H_1' + H_1'' + \ldots$$

Here, a_k and $a_k^\dagger$ are annihilation and creation operators of <u>acoustic</u> phonons in the kth mode. ω_k is their frequency, and C and D are the linear and quadratic crystal field coupling operators respectively (which operate on electronic states of the ion only), M is the mass of the crystal, and v is an average sound velocity in the crystal. Since this assumes the Debye approximation, v is assumed independent of $\vec{k}$ and $k = \omega_k/v$. For the typical energy level configuration, the relaxation transition probability for the ith level, due to the direct, single phonon process (W_i^d) is (using Yen's notation)

$$W_i^d = \frac{2\pi}{2Mv^2 \hbar} \left\{ \sum_{j < i} \omega_{ij} \rho(\omega_{ij}) |<A_j |C| A_i>|^2 \right.$$

33

$$[p_o(\omega_{ij}) + 1] + \sum_{j>i} \omega_{ij} \, \rho(\omega_{ij}) \, |<A_j|C|A_i>|^2 \, p_o(\omega_{ij}) \}$$

$$= \pi \left\{ \sum_{j<i} \beta_{ij} \, [p_o(\omega_{ij}) + 1] + \sum_{j>i} \beta_{ij} \, p_o(\omega_{ij}) \right\}.$$

Here, $\rho(\omega_{ij})$ is the detailed Debye density of states at ω_{ij}, and $p_o(\omega_{ij})$ is the phonon occupation number for phonons of energy $\hbar(\omega_{ij})$ at temperature T.

The contribution to the relaxation process due to Raman scattering of phonons by the impurity ion is calculated using H'_1 in second order and H''_1 in first order. This results in an expression for the ith level given by

$$W_i^R = \frac{2\pi}{\hbar} \, \bar{\alpha}_i \, (T/\theta_D)^7 \int_0^{\theta_D/T} dx \, \frac{x^6 e^x}{(e^x - 1)^2}$$

$$= \frac{2\pi\bar{\alpha}_i}{\hbar} \, (T/\theta_D)^7 \, \xi_6 \, (\theta_D/T),$$

where $x = \hbar\omega/kT$ and

$$\bar{\alpha}_i = \left(\frac{1}{k\,\theta_D}\right) \left\{ \alpha_i^2 + \frac{9 \, \hbar^2}{8 \, \pi^4 \, \rho^2 \, v^{10}} \left(\frac{k\,\theta_D}{\hbar}\right)^8 \left[\sum_{j \neq i} |<A_j|D|A_i>|^2 \right. \right.$$

$$\left. \left. + \sum_{i \neq j \neq k} \frac{|<A_j|C|A_k>|^2 |<A_k|C|A_i>|^2}{E_{jk} \, E_{ki}} \right] \right.$$

$$\alpha_i = \frac{3 \, \hbar}{2 \, \pi^2 \, \rho \, v^5} \left(\frac{k\,\theta_D}{\hbar}\right)^4 \left[<A_i|D|A_i> - \sum_k \frac{|<A_k|C|A_i>|^2}{E_{ik}} \right].$$

where θ_D is the Debye temperature (which turns out to be unrelated to the values consistent with bulk data such as specific heat). The integral $\xi_6(\theta_D/T)$ has been tabulated by Ziman and is proportional to $(\theta_D/T)^5$ at high temperatures.

The treatment of inhomogeneous strain broadening and homogeneous multiphonon relaxation broadening is essentially identical with that presented earlier. For the ith level, the total contribution to the linewidth due to H_1 is, therefore, given by Yen to be

$$\Delta\nu_i = \sum_{j<i} K_{ij} + \pi \sum_{j<i} \beta_{ij} \, [p_o(\omega_{ij}) + 1]$$

$$+ \pi \sum_{j>i} \beta_{ij} \, p_o(\omega_{ij}) + \frac{2\pi \, \bar{\alpha}_i}{\hbar} \, (T/\theta_D)^7 \, \xi_6 \, (\theta_D/T) \ .$$

34

where K_{ij} is the (essentially) temperature independent multiphonon contribution. For a given optical transition, the Lorentzian contributions from each level add

$$\Delta\nu_{ij} = \Delta\nu_i + \Delta\nu_j.$$

The contributions from the Gaussian shaped strain broadening are then added to $\Delta\nu_{ij}$.

The fit of this theory to experiment is difficult. Since only $\Delta\nu_{ij}$ is actually measured, the linewidth-vs-temperature curve must be measured for <u>all</u> optical transitions to separate out $\Delta\nu_i$ from $\Delta\nu_j$ and, hence, the various multiplicative coefficients (β_{ij}, α_i, and K_{ij} for <u>each</u> level). In addition to this, an elaborate fitting technique must be used to determine the proper value for θ_D. In general, a multiparameter fit requiring various β's and α's as variables is employed and these parameters are adjusted until a good fit is obtained. For example, in the case of the $^3P_0 \rightarrow (^3H_6)_{1, 2, 3}$ transition of P_r^{+3} in La F_3, Yen was able to reduce the number of coefficients from 6 to 3, before beginning the parametric fit (which depends on the dramatically different temperature dependencies of the direct and Raman processes). The fit to experiment is excellent.

The objective of the Debye theory is not to predict the shape of linewidth-vs-temperature curve for RE ions in crystals, nor is it to formulate an analytic expression for linewidth-vs-temperature, but rather to check the validity of the proposed broadening mechanisms themselves (direct phonon, Raman, etc). The success of demonstrating this has been excellent. The tradeoff is that the theory has four constraints relating to its utility of being a means of predicting the shape of the linewidth-vs-temperature curve with only a few measured points: the theory of Yen uses the Debye theory which is not valid for most hosts (where optical phonons interact strongly with the impurity ion) and requires complicated curve fits to determine an effective θ_D different from the results of bulk measurements; the functional expression for the Raman contribution is an integral form resulting in a nonanalytic expression; the Yen theory requires the measurement of many points on many linewidth-vs-temperature curves to enable the complicated parametric fit to be completed; and finally, the theory just does not "predict" the slope of the curves. The theory to be presented will address the prediction of the shape of the linewidth-vs-temperature curve for rare-earth impurity ions residing in hard crystals. Since data are available, and because of its wide application as a laser medium, Nd^{+3} YAG will be investigated specifically. The regime of $300°K$ to $400°K$ is of special interest as this is the typical operating temperature of high-power Nd^{+3} YAG lasers and amplifiers. The practical utility of a simple expression for the thermal dependence of linewidth requiring only the measurement of the $300°K$ linewidth and the low-temperature intercept for each optical transition desired is obvious.

EFFECTIVE MODE LINEWIDTH THEORY

RAMAN EFFECT OVER ALL MODES

The incorporation of all the preceding quantum electronic formalism into a theory to determine the thermal variation of the homogeneously broadened radiative transitions used in the operation of RE lasers requires the determination of the nonradiative energy level exchange rate between all sets of levels via all mechanisms. This requires that the fundamental dependence of linewidth-vs-temperature incorporating all effective modes for each mechanism must be found, the detailed set of energy levels must be examined to find all groups of interacting levels, and those mechanisms which can be neglected must be determined. By utilizing

the new approximation for interacting modes, for example, the predominant broadening mechanism (in Nd^{+3} YAG) will be shown to be the Raman type and an expression will be derived for the total nonradiative transition rate due to the summation of all effective modes. This will also set a practical limit for the maximum separation of energy levels connected via the Raman process. An expression will then be derived for the elastic Raman scattering process which homogeneously broadens an individual level independent of all others. This will turn out to be a very important mechanism and will greatly simplify the analytic expression used for the thermal variation of linewidth.

It is very important, though, to remember that the results to be presented are not applicable to ion-host laser systems in general. In fact, even the same rare-earth ion in another crystal may fall into regimes not accurately described by these approximations (neither qualitatively nor quantitatively). The system of Nd^{+3} YAG when used as a laser medium assumes, among other things, a RE ion (of small spatial extension causing low mixing of electronic and vibrational wave functions) located in small quantities (reducing ion-ion interactions) in a single crystal (low impurity levels to form perturbation centers) with a large unit cell (eliminating acoustic mode effects) in a "hard" crystal (allowing large-frequency phonons to interact with the ion). Also, the extremely low site symmetry without inversion relaxes most selection rules and a system with the impurity ion having an atomic weight much larger than its neighboring ions simplifies the vibrational structure. So, while the theory to be presented here can probably be modified to satisfy the general case of an ion-host combination, rederivation from fundamentals may be necessary.

First, the functional expressions must be found for the Raman broadening term, summing the effects for all active modes. The upward and downward Raman nonradiative transition rates between two energy levels separated by ΔE are given by the familiar relations (inelastic phonon scattering)

$$W_u^R = C\, n(\omega_1)\, [n(\omega_2) + 1]\, D'(\omega_1)\, D'(\omega_2)$$

with

$$W_d^R = C\, n(\omega_2)\, [n(\omega_1) + 1]\, D'(\omega_1)\, D'(\omega_2),$$

with $\omega_1 - \omega_2 = \Delta E$ (note figure 9). If all processes within the operation of this system as a laser occur with much larger time constants than the nonradiative exchange rate ($\sim 10^{-11}$ sec), then it may be assumed that the levels are always in thermodynamic equilibrium and described by Boltzman statistics. Therefore, W_u^R and W_d^R are not independent. Notice that this approximation breaks down when laser mode locking occurs (with pulse widths 10^{-12} sec) and when the level separation becomes large and the nonradiative exchanges are no longer described by a first-order effect; eg, by multiphonon effects. The equilibrium of the $4I_{11/2}$ thermal level and the $4I_{9/2}$ ground state is a two-phonon process with a relaxation time of approximately 0.5×10^{-6} second and, therefore, in the dynamic operation of a Q-switched laser ($\tau \sim 10^{-9}$ sec), these levels are far from remaining in thermodynamic equilibrium. But for all the first-order broadening mechanisms

$$W_d = e^{\Delta E/kT}\, W_u. \tag{45}$$

where ΔE is the energy level separation between the upper and lower states at T. If the equilibrium occupation numbers are substituted into the Raman relations above, the following is obtained (noting that $n(\omega) + 1 = n(\omega) e^{\hbar\omega/kT}$):

$$W_d^R = C \frac{1}{\alpha - 1} \frac{\alpha\beta}{\alpha\beta - 1} D'(\omega_2) D'(\omega_2 + \frac{\Delta E}{\hbar})$$

with

$$\alpha = e^{\hbar\omega_2/kT} \quad \beta = e^{+\Delta E/kT} \tag{46}$$

$$W_u^R = C \frac{1}{\alpha - 1} \frac{\alpha\beta}{\alpha\beta - 1} D'(\omega_1) D'(\omega_1 - \frac{\Delta E}{\hbar})$$

with

$$\alpha = e^{\hbar\omega_1/kT} \quad \beta = e^{-\Delta E/kT}. \tag{47}$$

Therefore, all that remains is to integrate the above expressions over all interacting modes to determine the contribution from all modes. If a detailed, highly structured expression for the effective density of states was used, it is clear that the above expressions would be sensitive to peaks in $D'(\omega)$ separated by ΔE. It is also clear that, for many such peaks in $D'(\omega)$, the results would tend to average to those obtained by employing a uniform effective density of states (the approximation to be used).

Before integrating the above, let us find the maximum energy-level separation, ΔE, connected by the Raman mechanism employing the uniform-density-of-states approximation. Here we normalize equation (44)

$$D'(\omega) = \begin{cases} 1 & \omega_{min} < \omega < \omega_{max} \\ 0 & \text{otherwise,} \end{cases}$$

where in this case $\omega_{min} = 250 \text{ cm}^{-1}$ and $\omega_{max} = 570 \text{ cm}^{-1}$. Note that $D'(\omega)$ is not integrable over all ω's to give three times the number of ions per unit cell, since these are only the effective modes. The Debye approximation normalizes in this manner and therefore considers all modes equally effective. Since it is always true that $\omega_1 - \omega_2 = \Delta E$, for W_d^R it must be that $\omega_2 > \omega_{min}$ in that $\omega_1 < \omega_{max}$ or $\omega_2 < \omega_{max} - \Delta E$. Therefore, for the example of Nd^{+3} YAG,

$$\Delta E < 320 \text{ cm}^{-1} \quad 250 \text{ cm}^{-1} < \omega_2 < 570 - \Delta E. \tag{48}$$

Therefore, at least to first order in our approximations, levels separated by over 320 cm^{-1} are not connected via the Raman mechanism and as $\Delta E \to 320 \text{ cm}^{-1}$ the quantity of effective modes interacting with the levels tends towards zero. For upward Raman transitions, again $\omega_1 - \omega_2 = \Delta E$ and since $\omega_2 > \omega_{min}$, $\omega_1 > \omega_{min} + \Delta E$ and $\omega_1 < \omega_{max}$, therefore

$$\Delta E < 320 \text{ cm}^{-1} \quad \omega_{min} + 250 \text{ cm}^{-1} < \omega_1 < 570 \text{ cm}^{-1}. \tag{49}$$

37

The range of values for ω_2 and ω_1 in equations (48) and (49) now specify the limits of integration in equations (46) and (47) for W_d^R and W_u^R.

As an example of how the structure of $D'(\omega)$ is used, consider the Stark doublet forming the upper lasing level in Nd^{+3} YAG – the $4F_{3/2}(2)$ and $4F_{3/2}(1)$ (note figure 5). Since the closest set of levels are the $4F_{5/2}$ (higher in energy by approximately $870\ cm^{-1}$), these two levels can be considered isolated and the nonradiative relaxation rates between them will determine the width of each level (neglecting elastic scattering for the moment). Since, from our approximation we find that $D'(88\ cm^{-1}) = 0$, the direct single-phonon transition rate is zero. Realistically, W^D is considered small and may be neglected (this will be discussed later). Therefore, the Raman expression alone defines the broadening of these levels. Using equations (48) and (49) the width of the $4F_{3/2}(2)$ level is given by

$$\Delta\nu[4F_{3/2}(2)] \cong \int_{\substack{\text{all} \\ \text{effective} \\ \text{modes}}} \frac{W_d^R}{\pi} + \Delta\nu\ \text{strain}$$

where Equation (46) is summed for $250\ cm^{-1} < \omega_2 < 482\ cm^{-1}$. Likewise,

$$\Delta\nu[4F_{3/2}(1)] \cong \int_{\substack{\text{all} \\ \text{effective} \\ \text{modes}}} \frac{W_u^R}{\pi} + \Delta\nu'\text{strain}$$

where equation (47) is summed for $338\ cm^{-1} < \omega_1 < 570\ cm^{-1}$. $\Delta\nu_{\text{strain}}$ is the inhomogeneous residual linewidth due to microscopic strain within the crystal. Properly, the Lorentzian shaped, Raman broadened line should not be added to the Gaussian strain line as linewidth is defined differently for each. The error will become more pronounced at low temperatures where $W^R \rightarrow 0$. Also, it should be noted that the two residual strain widths need not be equal.

The integration of equation 44 and 45 is straightforward. Using equations (48) and (49), the following is obtained:

$$W_d^R = C \int_{\omega_{min}}^{\omega_{max} - \Delta E} \frac{1}{\alpha - 1}\ \frac{\alpha\beta}{\alpha\beta - 1}\ d\omega$$

$$W_u^R = C \int_{\omega_{min} + \Delta E}^{\omega_{max}} \frac{1}{\alpha - 1}\ \frac{\alpha\beta'}{\alpha\beta' - 1}\ d\omega$$

where $\alpha = e^{\hbar\omega/kT}$, $\beta = e^{+\Delta E/kT}$, $\beta' = e^{-\Delta E/kT}$. Now all information on densities of states is incorporated into the limits. Since W_d is related to W_u by the Boltzman equation (equation 45), let us just integrate W_u^R.

If

$$\alpha = e^{\hbar\omega/kT} \text{ then } d\alpha = \frac{\alpha\hbar}{kT} \, d\omega,$$

so

$$W_u^R = \frac{C \, kT \, \beta}{\hbar} \int_{\omega_{min} + \Delta E}^{\omega_{max}} \frac{1}{\alpha - 1} \frac{1}{\alpha\beta - 1} \, d\alpha,$$

with primes eliminated and $\beta = e^{-\Delta E/kT}$. This expression becomes

$$W_u^R = \frac{C \, kT \, \beta}{\hbar} \int_{\omega_{min} + \Delta E}^{\omega_{max}} \frac{d\alpha}{\beta\alpha^2 + 2 \left[- \frac{(\beta + 1)}{2} \right]\alpha + 1} \tag{50}$$

which is in the form

$$\int \frac{dx}{A + 2Bx + Cx^2},$$

with

$$A = +1, \, B = \frac{-(\beta + 1)}{2}, \, C = \beta.$$

The following results depend upon

$$AC < B^2, \quad \text{or} \quad \beta < \left(\frac{\beta + 1}{2}\right)^2.$$

This is seen to always hold as the above reduces to $\beta^2 > 2\beta - 1$ and since $0 < \beta < 1$ ($\Delta E \geqslant 0$), this condition is always satisfied. Therefore the integration results in

$$\frac{1}{2\sqrt{B^2 - AC}} \ln\left[\frac{Cx + B - \sqrt{B^2 - AC}}{Cx + B + \sqrt{B^2 - AC}}\right].$$

So substituting for A, B and C in equation (50) and simplifying, the above expression becomes

$$W_u^R = \frac{C \, kT \, \beta}{\beta - 1} \ln\left[\frac{\beta\alpha - \beta}{\beta\alpha - 1}\right]\Bigg|_{\omega_{min} + \Delta E}^{\omega_{max}}. \tag{51}$$

If the limits are included and the expressions for α and β substituted, the following final result is obtained:

$$
W_u^R = \frac{C\,kT}{1 - e^{\Delta E/kT}} \, \ln\left[\frac{e^{(\hbar\omega_{max} - \Delta E)/kT} - e^{-\Delta E/kT}}{e^{(\hbar\omega_{max} - \Delta E)/kT} - 1}\right.
$$

$$
\left.\frac{e^{\hbar\omega_{min}/kT} - 1}{e^{\hbar\omega_{min}/kT} - e^{-\Delta E/kT}}\right]. \tag{52}
$$

W_d^R, when integrated over the proper limits, is given by $e^{\Delta E/kT}$ times W_u^R

$$
W_d^R = \frac{C\,kT}{e^{-\Delta E/kT} - 1} \, \ln\left[\frac{e^{(\hbar\omega_{max} - \Delta E)/kT} - e^{-\Delta E/kT}}{e^{(\hbar\omega_{max} - \Delta E)/kT} - 1}\right.
$$

$$
\left.\frac{e^{\hbar\omega_{min}/kT} - 1}{e^{\hbar\omega_{min}/kT} - e^{-\Delta E/kT}}\right]. \tag{53}
$$

Expressions (52) and (53) are analytic expressions requiring only the determination of the multiplicative parameter C (through fit to a single temperature) to determine the functional dependence of the Raman transition rate with temperature.

RAMAN ELASTIC PHONON SCATTERING APPROXIMATION

The elastic scattering of phonons from the impurity RE ion also induces a homogeneous broadening of that level. Rather than being an independent broadening mechanism, this process may be thought of as lifetime broadening due to the nonradiative transition rate between two levels whose energy separation is zero. In fact, since all levels in Nd^{+3} YAG are twofold Kramer degenerate, elastic scattering may be thought of as inelastic scattering between levels whose separation approaches zero. The expressions derived in equations (54) and (55) may be used to determine the individual width of a single level by looking at the limit as $\Delta E \rightarrow 0$. Contributions to the Raman component of linewidth broadening will come from $\Delta E = 0$ as well as from ΔE equal to energy level separations to adjacent Stark levels. Employing equation (51), it is seen that

$$
\lim_{\Delta E \rightarrow 0} W_u^R = \lim_{\Delta E \rightarrow 0}\left[\frac{C\,kT\,\beta}{\beta - 1} \, \ln\frac{\beta\alpha - \beta}{\beta\alpha - 1}\right]\Bigg|_{\omega_{min} + \Delta E}^{\omega_{max}} \rightarrow \frac{0}{0}.
$$

Therefore, l' Hospital's rule is employed and

$$\lim_{\Delta E \to 0} W_u^R = \frac{-C\, kT}{\hbar} \left(\frac{1}{\alpha - 1} \right) \Bigg|_{\omega_{min}}^{\omega_{max}}$$

Since elastic scattering involves only one level, W_u^R and W_d^R are replaced by a single rate of very simple functional form

$$W^R(T) = \frac{C\, kT}{\hbar} \left[\frac{1}{e^{\hbar\omega_{min}/kT} - 1} - \frac{1}{e^{\hbar\omega_{max}/kT} - 1} \right]. \tag{54}$$

Notice that this can be written very simply in terms of phonon occupation numbers as

$$W^R(T) = \frac{C\, kT}{\hbar} \left[n(\omega_{min}) - n(\omega_{max}) \right]$$

and that, at high temperatures, $W^R \propto T^2$, which agrees with the limit obtained using the Debye approximation.

Rather than requiring both forms of the Raman transition rate, an approximation will be employed which will greatly simplify the actual determination of linewidth-vs-temperature for a general set of Stark levels. This approximation is to employ only W^R for the Raman broadening component of a level. Consider figure 1, the energy level diagram for a general RE ion in a crystal. If the Raman contribution to the broadening of the ith level is desired, say, the following is found:

$$\Delta\nu_i^R = \frac{1}{\pi} \left[\gamma_i\, W^R(i) + \Sigma_\alpha \gamma_{i\alpha}\, W_u^R + \Sigma_\beta \gamma_{i\beta}\, W_d^R \right],$$

where γ_i is a multiplicative factor related to the magnitude of the contribution from elastic scattering (related to matrix elements), W_u^R is the upward Raman transition rate from the ith level to the αth level with a magnitude $\gamma_{i\alpha}$ (this is related to C in Equation (50)), and W_d^R is the downward transition rate from the ith level to the βth level with a magnitude $\gamma_{i\beta}$. The sums extend over all levels above (W_u^R) and all levels below the ith level with $\gamma_{i\alpha} = \gamma_{i\beta} = 0$ for $\Delta E > 320$ cm^{-1}. Since the quantitative factors $\gamma_{i\alpha}$ and $\gamma_{i\beta}$ are impossible to determine without precise knowledge of the matrix elements, and since their value is not expected to vary drastically with the wave functions used within a multiplet, all the $\gamma_{i\alpha}$'s and $\gamma_{i\beta}$'s are assumed equal. If this is assumed, a curve of W_u^R vs ΔE is plotted (for a particular T) and an estimate of the relative contributions of each mechanism can be obtained. Figure 13 shows W_u^R vs ΔE for T = 300°K and T = 100°K. Both show substantial reductions in the contribution of W_u^R vs W^R for typical values of ΔE — say, $\Delta E \sim 100$ cm^{-1}. Also, for $\Delta E < 150$ cm^{-1}, plots of W^R vs T and W_u^R vs T differ by less than 10 percent. Therefore, for $\Delta E <$ about 150 cm^{-1} the difference of $\Delta\nu$ vs T using the two methods is lower than experimental accuracy and for $\Delta E >$ 150 cm^{-1} the contribution of interlevel Raman broadening is considered small. The expression for
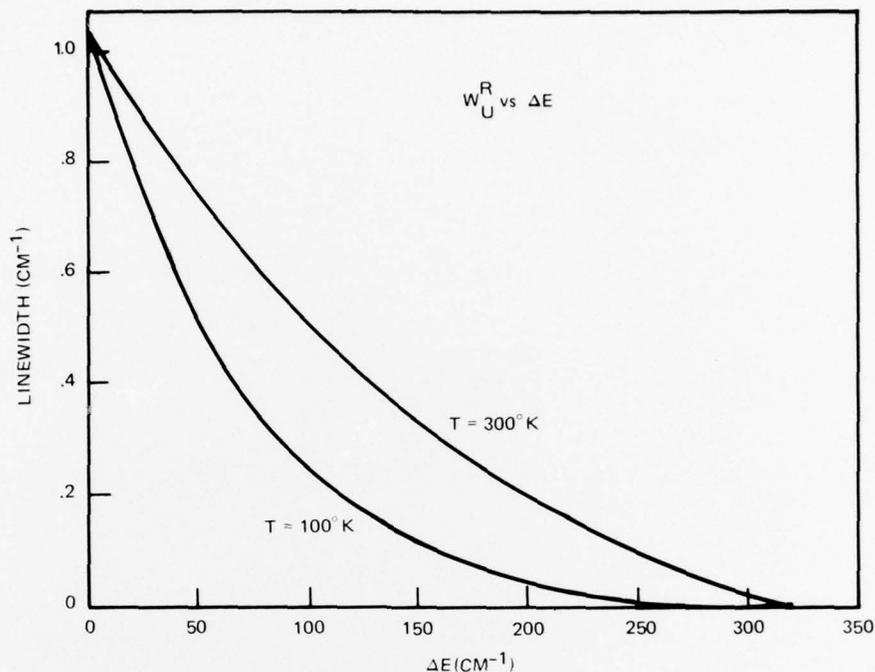
41

Figure 13. The upward Raman nonradiative transition rate (W_u^R) vs energy-level separation ΔE for temperatures of $100°K$ and $300°K$.

elastic Raman scattering W^R given in equation (54) will be used to determine the temperature dependence of the Raman two-phonon contribution to linewidth. Again, as with most approximations made, the quality of the predicted fit to the experimental results will indicate the validity of the approximations made. In addition to this recent assumption, many approximations and assumptions were made to derive the expressions for the Raman transition rate: complete local thermodynamic equilibrium; a uniform density of states described by the internal mode approximation with limited ranges (ie, equation (44)); and a completely first-order description of lattice phonons which neglects anharmonics and other higher-order effects which obscure crystalline wave functions and induce mixing of electronic and lattice wave functions, induce an appreciable phonon mode broadening, and generally destroy first-order theories as ionic displacements become large due to elevated temperatures.

DIRECT TRANSITION

Since the width of a typical energy level is much smaller than $D'(\omega)$ (approximately $3 \ cm^{-1}$ vs $300 \ cm^{-1}$), the expressions for the direct phonon mechanisms are governed by resonant transitions,

$$W_u^D = C'n(\omega) \, D'(\omega) \, \delta(\hbar\omega - \Delta E)$$

$$W_d^D = C'[n(\omega) + 1] \, D'(\omega) \, \delta(\hbar\omega - \Delta E).$$

42

Therefore,

$$W_u^D = \frac{C' \; 1}{e^{\Delta E/kT} - 1} \; D'(\Delta E/\hbar), \tag{55}$$

$$W_d^D = \frac{C' \; e^{\Delta E/kT}}{e^{\Delta E/kT} - 1} \; D'(\Delta E/\hbar), \tag{56}$$

with $D'(\Delta E/\hbar)$ given by the normalized equation (44). For $\Delta E < \omega_{min}$ and $\Delta E > \omega_{max}$, $W_u^D = W_d^D = 0$ (more properly, W^D becomes negligible). This greatly reduces the contribution of W^D to level broadening since the expressions are governed by phonon occupation numbers $n(\omega)$ which are large for small $\Delta E/kT$, consequently, $D'(\Delta E/\hbar)$ tends to render the upward direct phonon process (W_u^D) ineffective for the regions of maximum effect — *low energy spacings* with large $n(\omega)$'s. Also, since most Stark levels are separated by less than $250 \; cm^{-1}$, few levels even fall in the range of $D'(\omega)$ (and can couple with the effective phonon via the direct mechanism). If $\Delta E > \omega_{min}$ and $\Delta E < \omega_{max}$, W^D is allowed, but $n(\omega)$ tends to be small at all but the highest temperatures and W_u^D remains relatively ineffective in broadening the levels. Notice also that for large temperatures, the Raman mechanism increases much more rapidly than the direct ($W^R \propto T^2$ as compared to $W_u^D \propto T$).

W_d^D, on the other hand, tends toward a constant (of unknown magnitude relative to other mechanisms) as $n(\omega)$ becomes small and therefore contributes little to the thermal variation of the linewidth, and could be lumped together with the temperature independent, strain induced linewidth. This temperature independent contribution to linewidth is then determined independently. For the above reasons, the temperature dependence of the direct phonon, nonradiative transition broadening mechanism is considered to be small when compared to the Raman process when determining the thermal variation of linewidth in a system of Nd^{+3} YAG. Since the multiphonon process is also small, the thermal broadening of two energy levels is assumed to be due to residual strain and the Raman process only. This becomes another assumption to be redeemed by the quality of fit to the experimental data (and does indeed break down).

In passing, one should note two important points. First, for large T's (above $400°K$ say), this approximation will begin to fail as modes between 250 and $570 \; cm^{-1}$ will become significantly populated. Therefore, in addition to the effects of anharmonics and other higher order effects, the high temperature fit is expected to degrade due to the assumption of small functional dependence of W^D. Second and most important, for some intermediate energy level spacings, the assumption of a single, uniform density of states, with limits of $250 \; cm^{-1}$ and $570 \; cm^{-1}$ becomes important. Here it was assumed that the next nearest-neighbor modes (approximately one order of magnitude smaller) from $75 \; cm^{-1}$ to $225 \; cm^{-1}$ were negligible. This assumption may prove invalid if very large matrix elements (reflected in C') occur. Unfortunately, prediction when extraordinarily large values of

$$a_{K, k\Gamma_r} \; or \; < \psi_f | \hat{V}'_K | \psi_i >$$

occur is extremely difficult. Therefore, the approximation will be used with the possibility that large errors may result when a breakdown of that approximation occurs.

43

COMPARISONS TO EXPERIMENTAL DATA

Since the quantity of experimental data on linewidth-vs-temperature is limited, only a few lines will be considered here. It is important to recall that a line shape will be predicted here and checked with the experimental results. Only normalization to room temperature and determination of the low temperature intercept are necessary. Using the tools developed above, consider first the transition in Nd^{+3} YAG of $4F_{3/2}(2) \rightarrow 4I_{11/2}(1)$ – the $R_2 \rightarrow Y_1$ transition. Referring to figure 5 showing the partial energy level diagram for Nd^{+3} YAG, the following is found for the general expression, before simplification, for the linewidth of the $R_2 \rightarrow Y_1$ transition:

$$\Delta \nu(R_2 \rightarrow Y_1) = \frac{1}{\pi}[W^R_{R_2} + W^R_{Y_1}] + \frac{1}{\pi}[W^R_{d21}(R) + \sum_{i=2}^{5} W^R_{uli}(Y)] +$$

$$+ \frac{1}{\pi}[W^D_{d21}(R) + \sum_{i=2}^{5} W^D_{uli}(Y)] + \frac{1}{\pi}W_{mp} + \Delta \nu_s(R_2)$$

$$+ \Delta \nu_s(Y_1), \tag{57}$$

where $W^R_{R_2}$ and $W^R_{Y_1}$ are the elastic Raman broadening terms for the R_2 and Y_1 levels respectively, $W^R_{d21}(R)$ is the downward Raman transition from R_2 to R_1, $W^R_{uli}(Y)$ is the upward Raman transition from Y_1 to Y_i ($i = 2 \rightarrow 5$), $W^D_{d21}(R)$ is the downward direct-phonon transition rate from R_2 to R_1, $W^D_{uli}(Y)$ is the upward direct-phonon transition rate from Y_1 to Y_i, W_{mp} is any multiphonon transition rate, $\Delta \nu_s(R_2)$ is the inhomogeneous random strain-induced broadening for the R_2 level and $\Delta \nu_s(Y_1)$ is the strain broadening for the Y_1 level. By using the approximations discussed above, combining the W^R_d and W^R_u terms into W^R terms, neglecting the direct W^D_u and W^D_d terms, and neglecting all multiphonon terms, the following is used as the expression for $\Delta \nu(R_2 \rightarrow Y_1)$:

$$\Delta \nu(R_2 \rightarrow Y_1) = \frac{1}{\pi}[W^R_{R_2} + W^R_{Y_1}] + \Delta \nu_s(R_2) + \Delta \nu_s(Y_1).$$

Furthermore, since the functional dependence with temperature of $W^R_{R_2}$ and $W^R_{Y_1}$ is identical (independent of E), and since $\Delta \nu_s(R_2)$ and $\Delta \nu_s(Y_1)$ are constants, the above expressions can be further reduced to the extremely simple expression

$$\Delta \nu(R_2 \rightarrow Y_1) = \frac{1}{\pi}W^R(R_2 \rightarrow Y_1) + \Delta \nu_s(R_2, Y_1). \tag{58}$$

Now all that is required is the magnitude of $W^R(R_2 \rightarrow Y_1)$ (related to the constant "C" in equation (54)) and $\Delta \nu_s(R_2, Y_1)$; rather than seventeen difficult to measure, coupled parameters necessary in equation (57). The number of unknowns has been reduced as low as possible without detailed determination of crystalline wave functions and matrix elements.

44

Since

$$\lim_{T \to 0} W^R = 0, \tag{59}$$

the measurement of $\Delta \nu(R_2 \to Y_1)$ at low temperatures determines the residual strain broadening

$$\Delta \nu(R_2 \to Y_1) \Big|_{T \to 0} \cong \Delta \nu_s(R_2, Y_1). \tag{60}$$

Therefore, by requiring measurement at another temperature and implicitly assuming that $\Delta \nu_s$ is independent of temperature (obviously violated at very high temperatures causing large ionic displacements) the linewidth-vs-temperature curve for the $R_2 \to Y_1$ line in Nd^{+3} YAG is predicted. For convenience, $300°K$ is presumed as a reference temperature and W^R in equation (58) is "normalized" to $300°K$. Formally, a coefficient, say a, is introduced and fixed by requiring that

$$\frac{1}{\pi} W^R(300°K) = 1, \tag{61}$$

or if the π is absorbed into the W^R term, then normalization to $300°K$ results in

$$W^R(T) = W'^R(T)/W'^R(300°K),$$

where $W'^R(T)$ is given by Equation (54). Therefore,

$$\Delta \nu(R_2 \to Y_1) = aW^R(T) + \Delta \nu_s$$

with

$$a = \Delta \nu(R_2 \to Y_1) \Big|_{300°K} - \Delta \nu_s. \tag{62}$$

For the $R_2 \to Y_1$ curve, the low temperature intercept is measured by Kushida[20] to be 0.8 cm^{-1} and the $300°K$ linewidth to be 5.3 cm^{-1}. Therefore, the following is predicted for the functional dependence with temperature of the $R_2 \to Y_1$ radiative transition:

$$\Delta \nu(R_2 \to Y_1) = 4.5 \text{ cm}^{-1} W^R(T) + 0.8 \text{ cm}^{-1}. \tag{63}$$

When Equation (63) is plotted and the experimental points given by Kushida[20] are included on the curve, this results in figure 14. The agreement is good and within the stated experimental accuracy of $\pm 10\%$. The fact that good agreement is achieved with such a simple expression (Equation (63) was plotted with a desk calculator) and after so many approximations, is gratifying. It is observed that the fit begins to degrade at about $400°K$ and almost 10% errors are seen at $470°K$. As stated earlier, errors at high temperatures are not unexpected. Since most higher order effects are dependent on the particular wavefunctions involved (eg. effects of anharmonics will naturally be very dependent on the spatial form of ionic wavefunctions), a prediction of when high-temperature errors are large is very difficult. It will be observed

45

later that better agreement at high temperatures is achieved with some levels than with others. Also, since the quality of the fit over the entire curve is particularly sensitive to the experimental accuracy of the measurement of linewidth at $300°K$ (and somewhat sensitive to the determination near $0°K$), if a large error occurs experimentally with the determination of the linewidth at $300°K$, the shape of the entire curve is affected. In conclusion, it can be said that the agreement between the theoretically predicted curve and the experiment was achieved to over $177°C$ higher than most Nd^{+3} YAG lasers operate).

Consider now the $R_1 \rightarrow Y_1$ transition. Proceeding in the same manner as used for the $R_2 \rightarrow Y_1$ transition, the low temperature intercept is measured to be 0.6 cm^{-1} and the $300°K$ point is 4.0 cm^{-1}. Therefore, using equation (60),

$$\Delta\nu(R_1 \rightarrow Y_1) = 3.4 \text{ cm}^{-1} \text{ W}^R(T) + 0.6 \text{ cm}^{-1}. \tag{64}$$

This result is plotted along with experimental points in figure 15 and again good agreement is realized. The maximum error — occurring at $445°K$ — is nine percent.

Another transition, for which data are available, is the primary laser line in Nd^{+3} YAG. This line is composed primarily of the $R_2 \rightarrow Y_3$ line but also has overlapped from the $R_1 \rightarrow Y_2$ (note figure 15). The width of this composite line-vs-temperature was measured by Bell Laboratories[17] and is used as the experimental data with which to determine the quality of fit to the theory. If no consideration is given to the fact that the laser line is actually composed of two Lorentzian lines, but the two measured parameters of the laser are used with equation (60), a remarkably good fit is obtained. From this data, the room temperature width is measured to be 8.0 cm^{-1} and the low temperature width is 0.5 cm^{-1}. The prediction according to equation (58) is plotted, along with the data point, in figure 16

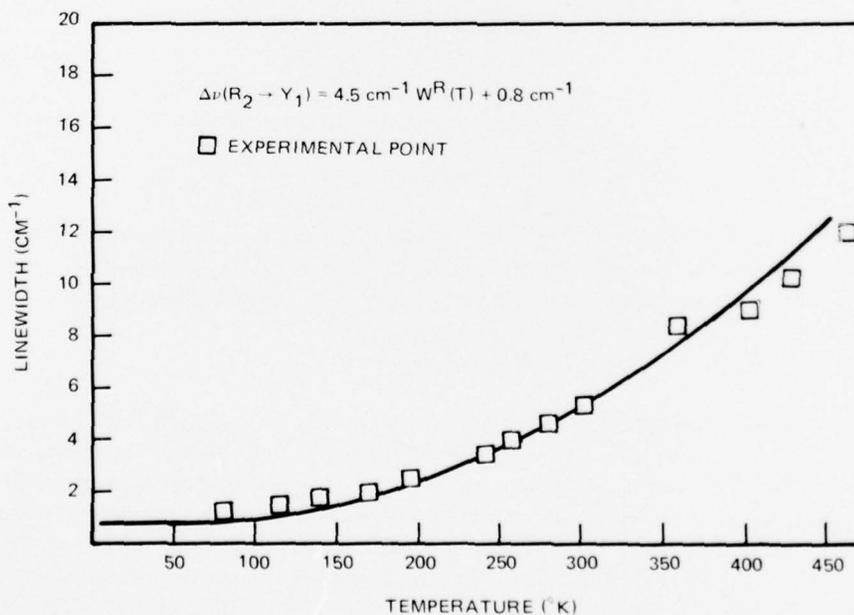$$\Delta\nu(\text{laser line}) = 7.5 \text{ cm}^{-1} \text{ W}^R(T) + 0.5 \text{ cm}^{-1}. \tag{65}$$

Figure 14. The theoretically predicted curve for the thermal dependence of the linewidth of the $R_2 \rightarrow Y_1$ radiative transition, showing experimental points given by Kushida.[18]
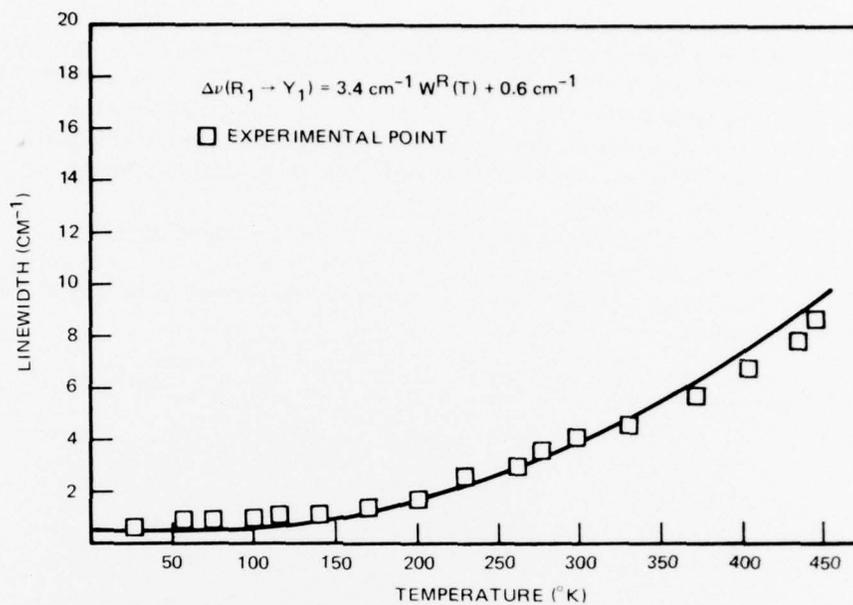
46

Figure 15. The linewidth-vs-temperature curve predicted for the $R_1 \rightarrow Y_1$ transition.[18]
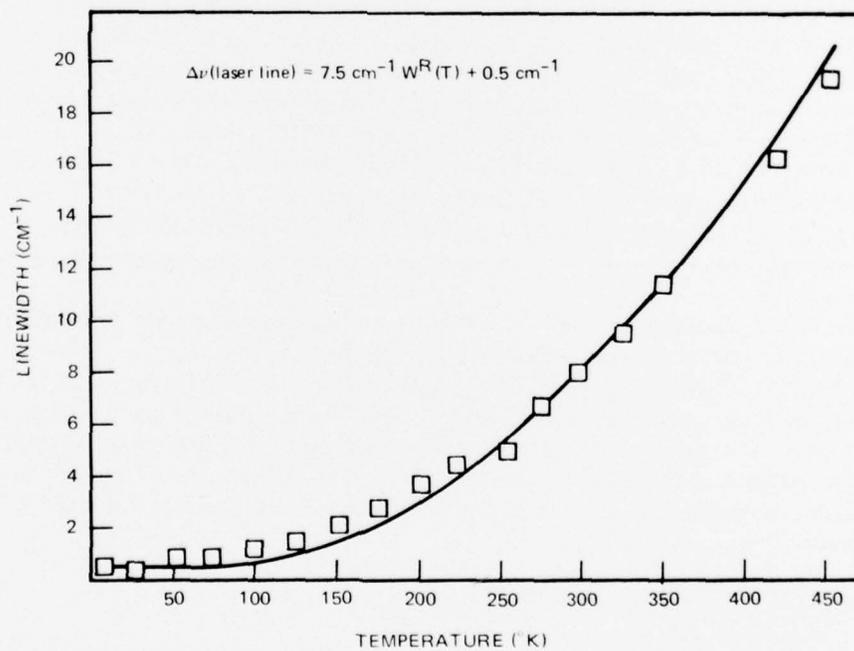

Figure 16. The linewidth-vs-temperature curve predicted for the composite laser line.[21]

Here, while good agreement is observed, a noticeable deviation occurs at about $150°K$ as well as the expected high-temperature error. The deviation around $150°K$ is attributed to the nature of the measurement of a "linewidth" composed of two Lorentzian lines of different magnitudes separated in wavelength added to a constant strain-broadened Gaussian line. Agreement becomes better at larger temperatures when the Lorentzian lines become much larger than the Gaussian lines.

In order to determine the transition cross-section and branching ratio for the laser line, Kushida, Marcos, and Geusic[20] decomposed the laser line into components of $R_2 \rightarrow Y_3$ and $R_1 \rightarrow Y_2$ (note figure 17). At "room temperature" (presumed to be $300°K$) the measured values were determined:

$$\Delta\nu(R_2 \rightarrow Y_3) \bigg|_{300°K} = 5.2 \text{ cm}^{-1}$$

and

$$\Delta\nu(R_1 \rightarrow Y_2) \bigg|_{300°K} = 4.2 \text{ cm}^{-1}$$

Notice that this correlates extremely well with the data for the $R_2 \rightarrow Y_1$ and $R_1 \rightarrow Y_1$ transition where linewidths of 5.3 cm^{-1} and 4.0 cm^{-1} were observed (the difference of 4.2 cm^{-1} to 4.0 cm^{-1} is 5 percent and within experimental accuracy). This implies, then, that the transitions from the R levels to the Y_1, Y_2 and Y_3 levels are broadened almost entirely by the R levels alone, and the contribution to the broadening due to the Y levels via any mechanism is small. This deduced fact is curious though unexplainable within the present scope. An attempt to explain why the $4I_{11/2}$ levels are not significantly thermally broadened, using the present development will not be attempted here. Therefore, the temperature dependence of the width of both the R_2 and R_1 levels has been explicitly determined and can be used in the R transitions to the Z levels, to be presented next. In passing, one might expect a similar correlation to be performed on the residual broadening at low temperatures. This would be meaningless, though, because different samples of Nd^{+3} YAG were used to perform the experiment and residual strain is a function of sample quality and can exhibit large deviations sample to sample.

The next radiative transition to be considered departs from the $R \rightarrow Y$ multiplets and is the transition from the $4F_{3/2}(1)$ level to the highest $4I_{9/2}$ level, the Z_5. Since the R_1 linewidth is already determined, all that is needed to determine the linewidth of the $R_1 \rightarrow Z_5$ transition is the temperature dependence of the Z_5 level. In practice, measurement of the width of a single level is not practical so the same procedure using equation (60) will be used with the preceding data from just R_1 used to establish the self-consistency of the theory. Here, the $300°K$ linewidth is found to be 9.25 cm^{-1} and the low-temperature intercept is 6.0 cm^{-1}. This results in

$$\Delta\nu(R_1 \rightarrow Z_5) = 3.25 \text{ cm}^{-1} \ W^R(T) + 6.0 \text{ cm}^{-1}. \tag{66}$$

which is plotted in figure 18 along with the experimental points. The agreement is generally good with deviation again being observed at high temperatures: 10-percent errors are

---

[20] T Kushida, H Marcos, and J Geusic, Physical Review, 167, 289, 1968

COMPOSITE LASER LINE

$\ell_2 : {}^4F_{3/2}(2) \rightleftharpoons {}^4I_{11/3}(3)$

$\ell_1 : {}^4F_{3/2}(1) \rightleftharpoons {}^4I_{11/2}(2)$

ℓ_2

ℓ_1

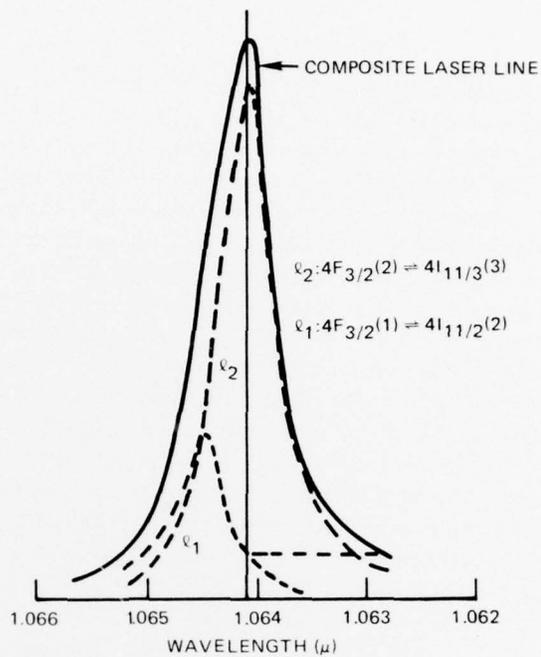1.066 1.065 1.064 1.063 1.062

WAVELENGTH (μ)

Figure 17. The emission spectrum of the 1.064μ "laser line" at room temperature showing the decomposition into $R_2 \rightarrow Y_3$ and $R_1 \rightarrow Y_2$ components.[16]
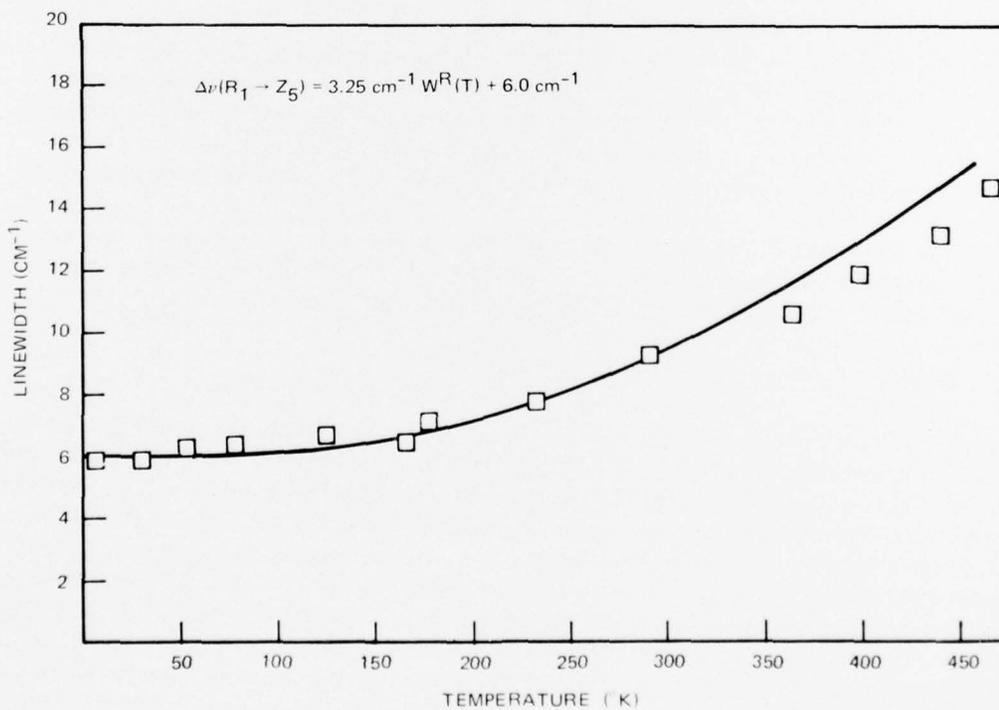

$\Delta v(R_1 \rightarrow Z_5) = 3.25$ cm^{-1} $W^R(T) + 6.0$ cm^{-1}

LINEWIDTH (CM^{-1})

TEMPERATURE (°K)

Figure 18. The linewidth-vs-temperature curve predicted for the $R_1 \rightarrow Z_5$ transition.[21]

[21] Solid-State Maser Research (Optical) Final Report, Bell Telephone Laboratories, US Army Electronics Material Agency, 30 August 1965

observed at $470°K$. Again, considering the approximations made to simplify the expression used in equation (60), and taking into account that this shape is "predicted" rather than least-square fit to the data, this fit is considered good. If the magnitude of the Raman term in the $R_1 \rightarrow Z_5$ transition (3.25 cm^{-1}) is compared with the previously determined value for just the R_1 level, 3.4 cm^{-1}, it is seen that here the width of the $R_1 \rightarrow Z_5$ transition is composed of the temperature-dependent Raman-broadened R_1 level and the temperature-independent Z_5 level. Actually, there is a contribution of the strain broadening from the R_1 level but it is small compared to 6.0 cm^{-1} (from equation (64) it is guaranteed less than 0.6 cm^{-1}). The self-consistency of this data is gratifying (the 5-percent discrepancy between the two values is within the experimental accuracy).

In the preceding section it was stated that the downward direct-phonon contribution to broadening was combined with the temperature-independent strain broadening because for most cases when $D'(\omega)$ is non-zero, $n(\omega) + 1 \rightarrow 1$ and is independent of temperature. Since it is really unimportant to the determination of the linewidth-vs-temperature curve what mechanism causes the residual broadening, all temperature-independent terms were combined. For the Z_5 level, an order of magnitude increase in the residual broadening is observed and some explanation is due. Here, the Z_5 level resides 537 cm^{-1} above the Z_4 level (figure 5) and is resonant with effective phonons contained in the lattice (within $D'(\omega)$). Since $n(537 \text{ cm}^{-1}) \ll 1$ at even $450°K$, this results in an estimate of what the coefficient for direct phonon transitions might be within the $4I_{9/2}$ multiplet (note that $Z_5 \rightarrow Z_3$ is outside $D'(\omega)$):

$$W_d^D (Z_5 \rightarrow Z_4) \cong 6.0 \text{ cm}^{-1} [n(537 \text{ cm}^{-1}/kT) + 1] D'(537 \text{ cm}^{-1}). \tag{67}$$

The coefficient of 6.0 cm^{-1} is of the same order as typical coefficients of the Raman expression — namely ~ 4 cm^{-1}. This direct-phonon coefficient is very large compared to the $R \rightarrow Y$ levels already examined since no large residual broadenings were observed. It will be shown later that the $4I_{9/2}$ levels do indeed exhibit extraordinarily large direct-phonon transition coefficients which result in a partial breakdown of the approximations used to derive equation (60).

The final curve for which data are available is the $R_1 \rightarrow Z_1$ transition. If the low temperature intercept is measured to be 0.5 cm^{-1} and the $300°K$ linewidth is measured to be 12.2 cm^{-1}, the following curve is derived using equation (60):

$$\Delta\nu(R_1 \rightarrow Z_1) = 11.7 \text{ cm}^{-1} W^R(T) + 0.5 \text{ cm}^{-1}. \tag{68}$$

If equation (68) is plotted, and data points entered, the curve in figure 19 is found. The fit is bad. At temperatures of about $150°K$, errors of 60 percent are observed and although data points are taken only to $320°K$, the slopes are seen to be radically different. This poor fit represents an obvious breakdown of certain approximations which were made. It will turn out that the source of error results because of the approximation as to the shape of $D'(\omega)$, wherein the low density of state phonons observed from 75 cm^{-1} to 250 cm^{-1} were ignored. The approximation was made to greatly simplify the analytic expression for W^R but becomes invalid when very large direct-phonon transition coefficients occur which more than offset the reduced magnitude of $D'(\omega)$ for $\omega < 250$ cm^{-1}. The quantum mechanics which explains why the $4I_{9/2}$ multiplets have an extraordinarily large coefficient is not understood and is beyond the present scope (eg, group theory will predict only qualitative effects; quantitative results require determination of matrix elements).

Incorporation of the direct phonon mechanism will now be pursued. As stated earlier, the R_1 level broadening is already determined and in fact, since the residual broadening of the R_1 level is almost identical to that of both the R_1 and Z_1 levels, all that is to be determined is the temperature-dependent level broadening of the Z_1 level. This level then will be both Raman and upward, direct phonon broadened. If the Raman broadening of the Z_1 level is assumed negligible, the upward phonon absorption mechanism remains, and the following can be deduced:

$$\Delta\nu(R_1) = 3.5 \text{ cm}^{-1} \text{ } W^R(T) + 0.5 \text{ cm}^{-1}$$

$$\Delta\nu(Z_1) = 8.2 \text{ cm}^{-1} \text{ } W_u^D \text{ (all levels),}$$

wherein

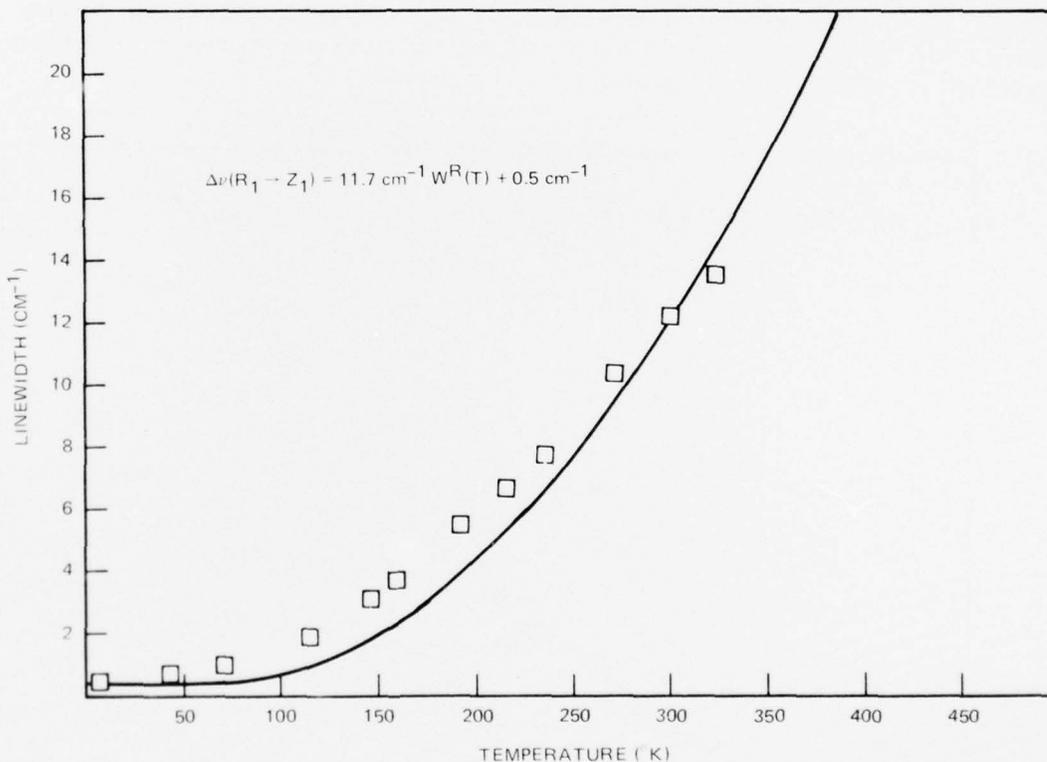$$W_u^D \text{ (all levels)}\bigg|_{300^\circ K} = 1.$$

Figure 19. The linewidth-vs-temperature curve predicted for the $R_1 \rightarrow Z_1$ transition, without the direct mechanism.[18]

51

If all multiplicative coefficients for the upward transition to each Stark level are assumed the same (there is no reason to assume this except for convenience), and if $D'(\omega)$ is assumed the same for all upward transitions (this is required because the detailed shape of $D'(\omega)$ fluctuates greatly), the following can be written for the linewidth of $R_1 \rightarrow Z_1$:

$$\Delta\nu(R_1 \rightarrow Z_1) = 3.5 \text{ cm}^{-1} \, W^R(T) + 8.2 \text{ cm}^{-1} \{ [n(134 \text{ cm}^{-1}; T) +$$

$$+ n(197 \text{ cm}^{-1}; T) + n(311 \text{ cm}^{-1}; T) + n(848 \text{ cm}^{-1}; T)] /$$

$$[n(134 \text{ cm}^{-1}; 300°K) + n(197 \text{ cm}^{-1}; 300°K) +$$

$$+ n(311 \text{ cm}^{-1}; 300°K) + n(848 \text{ cm}^{-1}; 300°K)] \} , \qquad (69)$$

where $n(\omega; T)$ is the occupation number of a phonon of frequency ω at temperature T. The plot of equation (68) and the data points is shown in figure 20 and excellent agreement is found. Again, the partial breakdown of the theory is not considered critical as the possible limits to the validity of the approximations were indicated, and also the tradeoff of simplicity, predictivity, and consistency is significant.
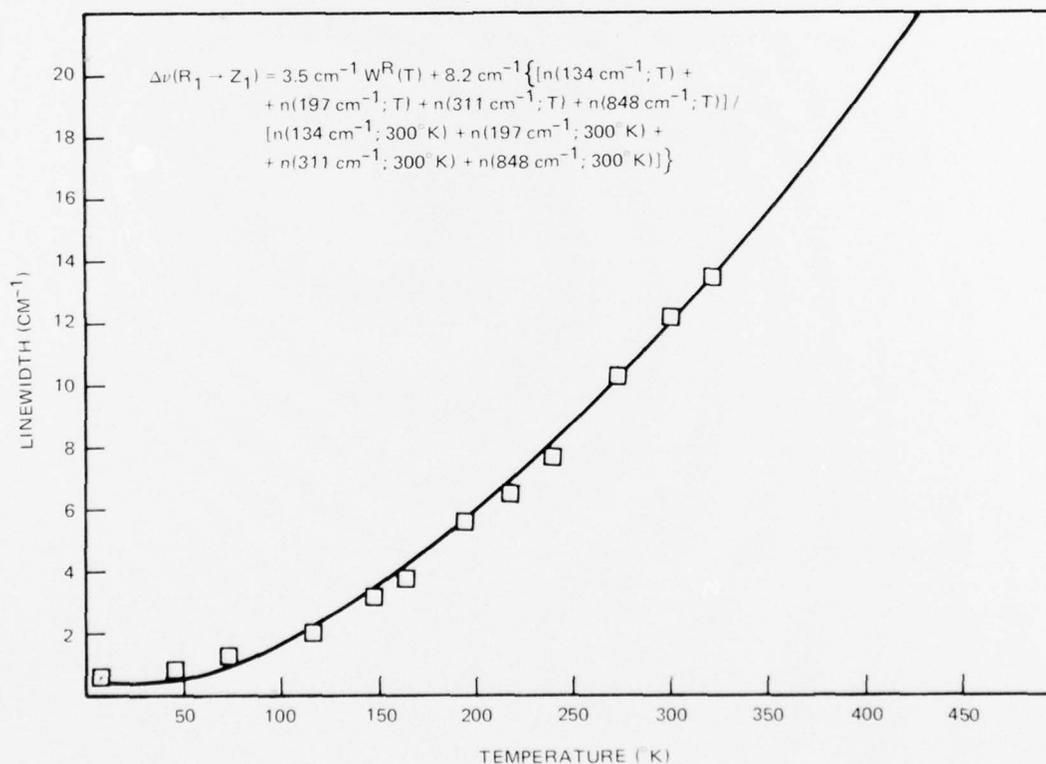

Figure 20. The linewidth-vs-temperature curve for the $R_1 \rightarrow Z_1$ transition obtained by employing the direct, single phonon mechanism.[18]

CONCLUSIONS

As stated in the Introduction, the objective of this technical report was to develop a simple compact theory to predict the shape of the linewidth-vs-temperature curves for Nd^{+3} YAG. This was to be done by accomplishing the following: establish the internal effective mode formalism necessary to model the ion-lattice interactions; determine a suitable approximation for the "effective" phonon spectra; by employing this approximation, derive compact, analytic, single multiplicative parameter expressions for the broadening mechanisms; determine the dominant broadening mechanism; and compare the predicted results with the experimental data. The previous theories had, as their objective, the verification of the validity of the proposed broadening mechanisms themselves (direct, Raman, strain, etc). The success at demonstrating this alone has been excellent. The constraints prohibiting the use of a Debye-based theory as a means of predicting the thermal variation of linewidth are four-fold: the theory of Yen employs the Debye theory for phonons which is not valid in most hosts (where the predominant ion-lattice interaction is via optical phonons) and requires a complicated curve-fit procedure to determine an effective θ_D (different from the results of bulk measurements); the functional expression for the Raman contribution is nonanalytic; it requires the measurement of many points on many linewidth-vs-temperature curves to enable the complicated parametric fit to be accomplished; and finally, and most significant, the theory of Yen does not "predict" the shape of the curve.

The internal mode theory presented here alleviates the above constraints. Here, an extremely simple expression, equation (58) is used to determine the thermal variations of linewidth for several optical transitions between multiplets of Nd^{+3} YAG (for which data were available). The $R_2 \rightarrow Y_1$ and $R_1 \rightarrow Y_1$ transitions fit well with the predictions; the expected high temperature degradation beginning at about $400°K$. This again is attributed to second-order lattice effects, experimental inaccuracies in the determination of the linewidth at $300°K$ and near $0°K$ used to determine the shape of the curve, and increasing thermal occupation of low energy modes resulting in small errors due to the approximation used for $D'(\omega)$ (ie, small contributions from the direct mechanism). Without even decomposition of the "laser line," the fit of this transition using equation (60) was excellent. In addition to the expected errors at high temperatures, the deviation around $150°K$ was attributed to errors resulting from adding two Lorentzian lines of different magnitude separated in wavelength added to a Gaussian line. The $R_1 \rightarrow Z_5$ transition also fits well with equation (58) but it was clear that the extraordinarily large residual broadening of 6 cm^{-1} is due to direct, spontaneous emission of phonons, since the energy gap to lower levels is within $D'(\omega)$. This is the first indication of extraordinarily large direct phonon coefficients for nonradiative transitions within the $4I_{9/2}$ multiplet. When the same procedure, using equation (60), was attempted for the $R_1 \rightarrow Z_1$ transition, very poor results were obtained. It is clear that, in this case, the direct phonon contribution cannot be neglected. When included, excellent agreement is again achieved. As stated before, the partial breakdown of some of the approximations is not considered critical, and indeed they were anticipated.

It can be stated that the objective of this theoretical analysis has been satisfied: a simple, compact internal mode theory predicting the shape of linewidth-vs-temperature curves for Nd^{+3} YAG has been developed.

REFERENCES

1. W Smith and P Sorokin, The Laser, McGraw-Hill Book Company, 1966

2. WM Yen, WC Scott, and AC Schawlow, Physical Review, 136, A271, 1964

3. DE McCumber and MD Sturge, Journal of Applied Physics, 36, 1682, 1963

4. A Kiel, Physical Review, 126, 1292, 1962

5. WD Portlow and HW Moos, Physical Review, 157, 252, 1967

6. CA Riseberg, WB Handrud, and HW Moos, Physical Review, 159, 262, 1967

7. CA Riseberg and HW Moos, Physical Review Letters, 19, 1423, 1967

8. CA Riseberg, HW Moos, and WD Portlow, Journal of Quantum Electronics, QE-4, 609, 1968

9. W Chang, Principles of Quantum Electronics, Addison-Wesley Publishing Company, Reading, MA, 1969

10. GS Ofelt, Journal of Chemistry and Physics, 37, 511, 1962

11. WF Krupke, Journal of Quantum Electronics, QE-7, 1953, 1971

12. JD Judd, Physical Review, 127, 760, 1962

13. BC Wybourne, Journal of Chemistry and Physics, 72, 639, 1960

14. IA Koningstein and JC Geusic, Physical Review, 136, A711, 1964

15. JC Prather, Atomic Energy Levels in Crystals, National Bureau of Standards Monograph 19, February 1961, US Government Printing Office, Washington, DC

16. M Tinkham, Group Theory and Quantum Mechanics, McGraw-Hill Book Company, New York, 1964

17. JH Van Vleck, Journal of Chemistry and Physics, 7, 72, 1939

18. T Kushida, Physical Review, 185, 500, 1969

19. RA Buchanan, Physical Review, 159, 245, 1967

20. T Kushida, H Marcos, and J Geusic, Physical Review, 167, 289, 1968

21. Solid-State Maser Research (Optical) Final Report, Bell Telephone Laboratories, US Army Electronics Material Agency, 30 August 1965

BIBLIOGRAPHY

EC Cohen and HW Moos, Physical Review, 1961, 258, 1967

A Kiel, Quantum Electronics III, Columbia University Press, New York, 1961

JP Hurrell and SP Porto, Physical Review, 133, 851, 1968

AH Ashbee and G Thomas, Journal of Applied Physics, 39, 3778, 1968

JH Van Vleck, Physical Review, 27, 425, 1940

GA Slack, Physical Review, 177, 1308, 1969

JM Ziman, Electrons and Photons, Oxford Press, 1962

C Kittel, Quantum Theory of Solids, John Wiley and Sons, New York, 1963

JM Ziman, Proceedings Royal Society of London, A226, 436, 1954